ORIGINAL RESEARCH ARTICLE

Microbial activity affects sulphur in biogenic aragonite

Vanessa Fichtner[1,2] (iD) | Skadi M. Lange[3] | Stefan Krause[3] | Thomas Huthwelker[4] | Camelia N. Borca[4] | Simon L. Schurr[2] | Adrian Immenhauser[5,6] | Chelsea L. Pederson[5] | Tina Treude[7,8] | Andrea M. Erhardt[9] | Harald Strauss[2]

[1]Institut für Geologie, Technische Universität Bergakademie Freiberg, Freiberg, Germany

[2]Institut für Geologie und Paläontologie, Westfälische Wilhelms-Universität Münster, Münster, Germany

[3]Department of Biogeochemistry, GEOMAR Helmholtz Centre for Ocean Research Kiel, Kiel, Germany

[4]Paul Scherrer Institut, Swiss Light Source, Villigen PSI, Switzerland

[5]Department of Geology, Mineralogy, and Geophysics, Ruhr-University Bochum, Bochum, Germany

[6]Fraunhofer IEG (Institution for Energy Infrastructures and Geothermal Systems), Bochum, Germany

[7]Department of Earth, Planetary, and Space Sciences, University of California, Los Angeles, Los Angeles, CA, USA

[8]Department of Atmospheric and Oceanic Sciences, University of California, Los Angeles, , Los Angeles, CA, USA

[9]Department for Earth and Environmental Sciences, University of Kentucky, Lexington, KY, USA

Correspondence
Vanessa Fichtner, Technische Universität Bergakademie Freiberg, Institut für Geologie, Bernhard-v.-Cotta-Straße 2, 09596 Freiberg, Germany.
Email: vae.fichtner@gmail.com

Abstract

Carbonates that exhibit obvious diagenetic alteration are usually excluded as archives in palaeoenvironmental studies. However, the potential impact of microbial alteration during early diagenesis is still poorly explored. To investigate the sensitivity of sulphur concentration, distribution, oxidation state and isotopic composition in marine aragonite to microbial alteration, *Arctica islandica* bivalves and *Porites* sp. corals were experimentally exposed to anaerobic microbial activity. The anoxic incubation media included a benthic bacterial strain *Shewanella sediminis* and a natural anoxic sediment slurry with a natural microbial community of unknown species. Combined fluorescence microscopy and synchrotron-based analysis of the sulphur distribution and oxidation state enabled a comparison of organic matter and sulphur content in the two materials. Results revealed a higher proportion of reduced sulphur species and locally stronger fluorescence within the pristine bivalve shell compared to the pristine coral skeleton. Within the pristine bivalve specimen, reduced sulphur was enriched in layers along the inner shell margin. After incubation in the anoxic sediment slurry, this region revealed rust-brown staining and a patchy S^{2-} distribution pattern rather than S^{2-}-layers. Another effect on sulphur distribution was rust-brown coloured fibres along one growth line, revealing a locally higher proportion of sulphur. The $\delta^{34}S$ value of carbonate-associated sulphate remained largely unaffected by both incubation media, but a lower $\delta^{34}S$ value of water-soluble sulphate reflected the degradation of insoluble organic matter by microbes in both experiments. No significant alteration was detected in the coral samples exposed to microbial alteration. The data clearly identified a distinct sensitivity of organically bound sulphur in biogenic aragonite to microbial alteration even when 'traditional' geochemical proxies such as $\delta^{18}O_{CARB}$ or $\delta^{13}C_{CARB}$ in the carbonate did not show any effect. Differences in the intensity of microbial alteration documented are probably due to inherent variations in the concentration and nature of original organic compositions in the samples.

KEYWORDS
carbonate diagenesis, carbonate-associated sulphate, microbial alteration, stable sulphur isotopes

1 | INTRODUCTION

Under favourable conditions, marine biogenic carbonates may serve as archives for their ambient seawater properties. Nevertheless, the environmental information encoded in these skeletal hardparts is often affected by metabolic effects and can undergo *post mortem* alteration. One of the many processes that affect this proxy data is microbial colonisation of skeletal hardparts and related metabolisms, a factor rarely addressed in previous work (cf. Glover & Kidwell, 1993; Lange et al., 2018; Sejrup & Haugen, 1994). These studies demonstrated that microbial activity has the potential to alter the elemental composition of these archives, and thus, can also affect any conclusions drawn regarding ambient seawater conditions.

Carbonate-associated sulphate (CAS) is a proxy to explore global sulphur cycling (Burdett et al., 1989; Gill et al., 2007; Kampschulte & Strauss, 2004). It is generally hosted in the mineral portion of the skeletal carbonates and substitutes for the carbonate ion (Staudt & Schoonen, 1995; Takano, 1985). However, CAS is not the only sulphur phase in biogenic carbonates (Cuif et al., 1999; Fichtner et al., 2018). Sulphur, for example, is also present in the organic compounds in marine biominerals as sulphated sugars, as reduced sulphur in amino acids and, in rather minor abundance, as sulphate esters and thiols (Dauphin, 2003; Dauphin et al., 2003; 2005; Perrin et al., 2017; Richardson et al., 2019). The sulphate fraction of the intra-shell soluble organic matter in *A. islandica* is extractable as water-soluble sulphate (WSS) and is characterised by a $\delta^{34}S$ value lower than the respective $\delta^{34}S$ value for CAS (Fichtner et al., 2018). Due to its presence in the intra-shell organics, sulphur is potentially an element indicative of microbial mining, that is, microbial activity with the aim to exploit the organic portions of these biominerals.

In the present study, shells of *Arctica islandica* and skeletal hardparts of *Porites* sp. were used to demonstrate the impact of microbial metabolic activity on sulphur in biogenic carbonates. Both samples consist of biogenic aragonite but differ significantly in their microstructure, organic content and porosity (Pederson et al., 2020). *Arctica islandica* is a marine bivalve from the Northern Atlantic with an endobenthic lifestyle (Schöne, 2013). Due to its value as a climate proxy and an unusually high longevity, *A. islandica* is the subject of numerous studies focussing on shell microstructure and chemistry (Karney et al., 2012; Pederson et al., 2019; Schöne, 2013; Schöne et al., 2010; Shirai et al., 2014). Corals of the genus *Porites* inhabit tropical shallow oceans and are frequently used as palaeo-archives of sea surface temperatures and sea-level fluctuations (Corrège, 2006; Fallon et al., 2002; Hendy et al., 2003; Marshall & McCulloch, 2002). Previous XANES (X-ray absorption near-edge structure) studies reported sulphur to be exclusively present as sulphate in coral skeletons (Cuif et al., 2003; Nguyen et al., 2014; Perrin et al., 2017; Tamenori et al., 2014).

This study compares the influence of microbial metabolic activity on the distribution, concentration and oxidation state of sulphur in biogenic carbonates. Aragonitic bivalve shells and coral segments were incubated in three anoxic media: (a) the marine benthic bacterial strain *Shewanella sediminis*, (b) a natural sediment slurry and (c) a sterile anoxic control. Combined sulphur XANES analyses, μ-XRF (X-ray fluorescence) element mapping, fluorescence and transmitted microscopy, and sulphur isotope analyses were conducted in order to investigate: (a) possible effects of microbial degradation on the concentration, distribution, oxidation state and sulphur isotope composition of sulphur compounds in biogenic aragonite, and (b) variations in the degree of microbial alteration of sulphur depending on the sample type. It is argued here that a detailed investigation of fluorescence images, distribution, oxidation states and isotopic composition of sulphur can aid in identifying changes in the concentration and composition of the organic components in biogenic carbonates, which in turn, can help assess the degree of microbial activity. Explanations for the different effects of microbial alteration in *A. islandica* and *Porites* sp. samples are discussed.

2 | SAMPLE MATERIAL AND METHODS

2.1 | Biogenic aragonite samples

Living *A. islandica* specimens were dredged from the sea floor north-east of Iceland at water depths of 40–120 m. Directly after sampling, the soft tissue was removed and the valves were mechanically cleaned, dried and stored in a dry and cool location. Remnants of the animal's flesh or different amounts of natural sediment on the shells would have made it challenging to compare geochemical parameters of the shell margins of the pristine and the incubated shell samples. Analysis of the pristine shell ultrastructure revealed no significant change in the intercrystalline organic matter after sampling (Casella et al., 2017). Bivalve shells were on average 10 cm in length. Subsamples $1 \times 1 \times 0.5$ cm in size were cut from the shells prior to the incubation experiments. The *Porites* sp. coral was sampled in vivo in the Gulf of Aqaba in the Red Sea, in 1993. Corals were mechanically cleaned, dried and stored at room temperature before the incubation experiments. Subsamples $1 \times 1 \times 2$ cm in size were cut for the incubation experiments.

2.2 | Incubation media and sample treatment

Incubation experiments were performed over a 3 month interval. For all incubations, natural North Sea seawater served

as the base for the incubation media, after being treated with UV light and filter-sterilised with a 0.2 μm filter (Whatman) to remove any particles from the fluid.

For the first incubation experiment, the *S. sediminis* bacterial culture was grown in an anoxic DSMZ (Deutsche Sammlung von Mikroorganismen und Zellkulturen) medium 514 (for medium composition see Lange et al., 2018). 10 ml of this fluid was added to 900 ml of the sterile seawater with an additional 100 mg/l Fe (III) citrate, 1,000 mg/l yeast, and 200 μl resazurin as a redox/oxygen indicator. *Shewanella sediminis* was chosen for the experiment due to its ubiquity in marine sediments and its ability to ferment *N*-acetyl-glucosamine (chitin; Zhao et al., 2005), which is an integral organic-matrix constituent of many marine calcareous structures (Marin et al., 2012; Weiner and Addadi, 1991). This ability allows for potential post-mortem alteration of marine carbonates by microbial de-stabilisation (fermentation) of the intercrystalline and intracrystalline organic matrix and for metabolic side effects, such as changes in trace-element concentration and isotope composition, that serve as palaeoenvironmental proxies. For the first confirmatory studies see Lange et al. (2018). The second experiment contained anoxic sediments collected at 17 m water depth in the German Bight, North Sea (54°50′N, 8°89′E), containing natural microbial communities. The slurry comprised 300 g of sediment and 600 ml of sterilised seawater. A third set of experiments served as a control, where pristine sample material was incubated in sterile anoxic seawater.

All media were poured into sterile 2 l gastight flange beakers with a N_2 headspace. Shell and coral samples incubated in the *S. sediminis* medium were fixed with sewing thread and suspended in the water column. Samples incubated in anoxic slurries were placed on the surface of the natural anoxic sediment. Experiments were conducted in the dark at a constant temperature of 10°C. Following the experiment, samples were removed from the experimental vessels, rinsed with seawater, and further rinsed with ultra-purified water with an adjusted pH 8 (by addition of NH_4^+) to prevent shell dissolution. The samples were subsequently dried at 40°C. A detailed description of the microbial incubation experiments used in this study was previously reported by Lange et al. (2018).

After drying, thick sections of the bivalve shells were cut parallel to the growth direction from the inner to the outer portion of the shell, and polished to a thickness of 100 μm. Thick sections of the coral samples were prepared from a cross-section from the outer to the central part of the skeleton without a particular orientation to the growth direction, and polished to a thickness of 100 μm. The fragile structure of both sample types prevented the sections being cut thinner than 100 μm. A Körapox 439 resin was used to mount the thick sections on glass slides.

2.3 | Sulphate extraction from *A. islandica* incubation media and isotope measurements

For the extraction of sulphate, 20 ml of fluid was sampled and filtered (0.2 μm, Whatman) from the sterilised seawater, the incubation fluid and the control fluid after the experiment. The fluid pH was adjusted to <2 using HCl (25%). The fluids were heated to 90°C and mixed with 2 ml of 10% $BaCl_2$, causing the dissolved sulphate to precipitate as $BaSO_4$. This was then separated from the fluid by filtration through a 0.2 μm cellulose-nitrate filter. Following drying at 40°C, the concentration of the dissolved sulphate was determined gravimetrically. No additional steps were taken to prevent oxidation of aqueous sulphide.

In total, 200 μg of the dried barium sulphate ($BaSO_4$) precipitates were mixed with *ca* 400 μg V_2O_5 for sulphur isotope analyses. A ThermoFinnigan Delta Plus mass spectrometer interfaced with an elemental analyser (EA-IRMS: Elemental Analyser-Isotope Ratio Mass Spectrometry) was used for isotope measurements. Sulphate oxygen isotopes ($\delta^{18}O_{SO4}$) were measured on 200 μg of the precipitated $BaSO_4$, using a ThermoFinnigan Delta Plus XL mass spectrometer interfaced with a high-temperature pyrolysis unit (Temperature Conversion/EA-IRMS). Results are reported in the standard delta notation as per mil differences to the V-CDT standard for sulphur isotopes ($\delta^{34}S$), and the V-SMOW standard for oxygen isotopes. International reference materials used for sulphur isotope measurements were IAEA-S1 (−0.3‰, V-CDT), -S2 (+22.62‰, V-CDT), -S3 (−32.49‰, V-CDT) and NBS 127 (+21.12‰, V-CDT), with reproducibility generally above 0.3‰. The $\delta^{18}O_{SO4}$ measurements had a reproducibility generally better than 0.5‰, and used international reference materials IAEA-SO5 (+12.13‰, V-SMOW), -SO6 (−11.35‰, V-SMOW) and NBS 127 (+9.34‰, V-SMOW). Values for the reference materials were taken from Brand et al. (2014).

2.4 | Sulphur isotope analyses and extraction of sulphate and intra-shell organic matter from *A. islandica* shells

Water-soluble sulphate and CAS were extracted from the pristine shell segment and from segments incubated in the *S. sediminis* culture and the anoxic sediment slurry following the techniques employed in Wotte et al. (2012). Powdered shells were rinsed three times with 10% NaCl solution for 24 hr each. Following the first rinse, sulphate from the solution was analysed for its WSS sulphur isotope value. To extract the CAS, the samples were subsequently dissolved in 25% HCl. The solutions (6 in total) were eluted through columns containing 2 ml of the anion exchange resin (AG®1-X8; Cl⁻ form; 200–400 mesh; BIORAD Labs). Prior to ion separation, the

resin was rinsed with 20 ml (3M) HNO_3, 20 ml (6M) HCl and 40 ml Milli-Q-water. After pouring the sample solution into the column the cations were washed out by rinsing the column three times with 5 ml Milli-Q-water. Thereafter, the anions were washed out by rinsing the column three times with 4 ml (0.5M) HNO_3. The sulphur isotope ($\delta^{34}S$) composition was measured using a Thermo Scientific™ Neptune Plus MC-ICPMS. Samples were introduced in 0.25 M HNO_3 solutions with an Apex-Ω desolvator (Elemental Scientific) using a Savillex® PFA nebuliser with a nominal uptake rate of 50 µl/min. Samples contained *ca* 1 ppm sulphate and full procedural blanks were between 25 and 83 ng sulphur. The long-term $\delta^{34}S$ reproducibility was 0.2‰. The standard deviation for a 1 ppm standard sulphate solution was between 0.5 and 1.4‰ (2 SD). Reported precisions of sulphur isotope measurements (see 2 SD in Table 1) include instrument stability, reproducibility of the same sulphate solution within an analytical session, and blank contribution during sample preparation.

The insoluble organic matter was separated from 20 g of non-incubated shell powder by dissolving the host carbonate in acetic acid. The residue was obtained via centrifugation of the sample in a falcon tube. It was then rinsed with distilled water and dried in an oven at 40°C. Between 160 and 350 µg of the dry intra-shell organic matter was placed into tin capsules and analysed for its sulphur isotope composition using a Thermo Scientific™ EA IsoLink™ IRMS.

All sulphur isotope results are reported in the standard delta notation as per mil difference to the V-CDT standard for sulphur isotopes ($\delta^{34}S$). For calibration to the V-CDT scale an independently calibrated sulphate standard solution (Merck®) with a $\delta^{34}S = 4.4‰$ (SD = 0.4‰, $n = 4$) was used as bracketing solution. For further details, please refer to Schurr et al. (2020) and Paris et al. (2014). The reproducibility was better than 1.0‰ for the MC-ICPMS analyses, and better than 0.3% for the EA-IRMS analyses.

2.5 | Microscopy

Reflected light images of the shell and coral thick sections were taken with a Canon eos 7D and an MP65 objective. A Leica DM4500 P LED microscope was used for fluorescence and transmitted light images. Fluorescence images were generated using the blue light spectrum (450–490 nm) for excitation.

TABLE 1 Sulphate concentrations and $\delta^{34}S$ and the $\delta^{18}O$ values of the incubation media, modern seawater sulphate and different sulphur phases from the *Arctica islandica* shell

	SO_4^{2-} (g/l)	$\delta^{34}S_{SO4}$ (‰, V-CDT)	SD	$\delta^{18}O_{SO4}$ (‰, V-SMOW)	SD
Incubation media					
Sterilised seawater	2.6	20.5	0.08	7.7	0.24
Control (anoxic seawater)	2.5	20.4	0.02	8.3	0.48
Anoxic sediment	2.6	18.3	0.04	10.0	0.23
Shewanella sediminis culture	2.6	20.5	0.15	9.0	0.53
Modern seawater	2.7	21.2	0.15	8.7	0.21
Arctica islandica shells					
CAS (pristine)		20.6	0.4		
CAS (pristine)		21.0*	0.1		
CAS (*S. sediminis*)		20.8	0.2		
CAS (anoxic sed.)		21.9	0.5		
WSS (pristine)		17.8	0.2		
WSS (pristine)		17.8*	0.1		
WSS (*S. sediminis*)		12.7	0.4		
WSS (anoxic sed.)		14.6	0.2		
Sulphur in insol. organics		10.7	0.4		

Note: The $\delta^{34}S$ and the $\delta^{18}O$ values of modern seawater sulphate were determined by Johnston et al. (2014). $\delta^{34}S$ values of sulphur in the shells were measured with MC-ICPMS except for those marked with "*". They were published in Fichtner et al. (2018) and measured with IRMS.

2.6 | Synchrotron analyses

Synchrotron analyses were performed at the PHOENIX (Photons for the Exploration of Nature by Imaging and XAFS) beamline at the Paul Scherrer Institut (PSI, Villigen, Switzerland). The PHOENIX beamline covers the energy range of 0.4 to 8 keV using two branchlines. The measurements shown here were carried out at the PHOENIX I branch (0.8–8 keV). The beamline closely follows the optical layout of the former LUCIA beamline (Flank et al., 2006). An APPLE II elliptical undulator briefly served as a light source. A double crystal monochromator (Bruker, AXS GmbH) which hosts four different sets of crystals created monochromatic light and was used for measurements. For the work presented here, the silicon (111) crystal was used. The X-ray beam was focussed to ca 3×3 μm using focussing X-ray mirrors (Kirkpatrick-Baez system). The intensity of the incoming beam was measured as a total electron yield (TEY) signal on a Ni coated polyester foil, located ca 1 m upstream of the sample, at ca 5×10^{-7} mbar of pressure. Fluorescence signals were collected using a detector with four elements of silicon drift diodes (Vortex, Hitachi, California 91311, USA).

2.6.1 | XANES analyses

X-ray absorption near-edge structure analyses of the sulphur K-edge were performed on the bivalve and coral thick sections using a focussed beam with a spot size of 4 μm^2. The beam energy ranged from 2,423 to 2,600 eV with a step size of 3 eV between 2,423 and 2,465 eV, 0.3 eV between 2,466 and 2,490 eV, 1 eV between 2,491 and 2,500 eV, and 2 eV between 2,501 and 2,600 eV. Different reference materials were used to calibrate the peaks to sulphur oxidation states. Inorganic reference materials used were $CaSO_{4*}$ $2H_2O$, $CaSO_4$, $SrSO_4$, Na_2SO_4 and $MgSO_4$. Organic reference materials were cysteine, cystine, methionine and chondroitin sulphate. Their sulphur XANES spectra were measured with an unfocussed beam (1 mm^2 size) as TEY and were previously described in Fichtner et al. (2018). The energy calibration was defined by the sulphate ($CaSO_4$) peak maximum, which was set to 2,482.3 eV (Supporting information). The more reduced the sulphur, the more the white line position shifted towards lower energies. For S^{4+} and S^{2-}, the additional peaks occurred at beam energies of around 2,477 and 2,472 eV (Supporting information; Perrin et al., 2017). Additional peaks and spectral features at energies above the K-edge reflected electronic transitions into continuum states, and most importantly the scattering of photoelectrons in the local environment. Hence, this part of the spectrum reflects the local coordination around the probed atom and can serve as a fingerprint to identify mineral and amorphous phases.

All XANES spectra were processed using the software ATHENA (Ravel & Newville, 2005).

2.6.2 | Micro-XRF mapping

Total sulphur and strontium μ-X-ray fluorescence mapping

Sulphur and strontium μ-X-ray fluorescence (μ-XRF) maps of the bivalve and coral samples were generated during two different measurement periods. The analyses of the coral control samples were limited to the pristine samples due to scheduling, whereas the analyses of the bivalve control samples included both the pristine shell and the shell incubated in sterile seawater. In a first round of measurements, the bivalve samples were analysed with a beam energy of 2,800 eV. In a later set of measurements, the coral samples were analysed with a beam energy of 2,600 eV. These beam energies enabled the detection of different XRF lines, including the sulphur and magnesium K lines and the strontium L lines. The lower beam energy of 2,600 eV was used for the coral thick sections to minimise any enhanced background below the sulphur emission line, which occur in a silicon drift diode, when peaks of heavier elements are present in the sample (e.g. chlorine from NaCl), or when stray light excites chlorine, which is abundant in the resin. For both sample types, a 5 μm step size was used to obtain the elemental maps, with a beam size of 4 μm. The μ-XRF maps of the bivalves ranged from 2,055 to 3,105 μm in length and 60–70 μm in width, and covered the cross-section from the inner to the outer shell rim. The μ-XRF maps of the corals were 500–570 μm in length and 150–200 μm in width, and covered the surface area directly exposed to the incubation medium and extended to the center of the subsample. The program PYMCA (Solé et al., 2007) was used for data processing. The maps obtained after the fitting were made for qualitative comparison of the samples and were not intended for an absolute measure of sulphur and strontium concentrations.

Sulphur oxidation states mapping

Smaller maps (150 × 40 μm on average) with a spatial resolution of 3 μm were generated to decipher any difference between the distribution patterns of S^{6+} and S^{2-} species along the inner shell surface of all *A. islandica* subsamples, and along the outer shell surface of the pristine *A. islandica* adjacent to the area where the total sulphur maps were created. To generate the maps, the Kα emission line (2,309 eV) was recorded using an energy-dispersive silicon drift detector. As these emission lines were reasonably isolated from emission lines of other elements, a complete peak fitting of the full XRF spectra (data not shown) was not necessary for the oxidation state mapping. Hence, regions of interest (ROIs) including only the raw signals from the sulphur Kα emission lines were manually selected from the

XRF spectra to generate the maps of the sulphur distribution for different excitation energies.

For these maps, the same area was analysed with four different excitation beam energies, commencing with the energy below the sulphur K-edge (2,464 eV), followed by the energy at the S^{2-} peak (2,472 eV), the energy at the S^{6+} peak (2,482 eV), and lastly the energy well above the absorption edge at 2,560 eV. Since the μ-XRF maps generated with a beam energy of 2,482 eV contain both the S^{2-} and S^{6+} distribution patterns in the Kα emission line, the maps taken at the lower energies were created in order to get distinct signals of the different sulphur oxidation states. The maps showing the distribution of S^{6+} and of S^{2-} were calculated from the measured, unprocessed maps. The map taken at 2,464 eV measured the magnitude of the height of the pre-edge contribution and needed to be subtracted from all other maps. The total amount of sulphur was measured by a map collected at 2,560 eV, well above the sulphur absorption edge, where sulphur is excited non-resonantly. This map was used to normalise all other maps to an edge step of 1. For the further analysis it was assumed that S^{6+} and S^{2-} are the dominant species in the bivalve shell samples which was confirmed by the point spectra form taken from the samples. To identify the regions with low and high S oxidation states, two additional maps were created at 2,472 and 2,482 eV. The 2,472 eV map excites only the S^{2-} oxidation state, but no higher oxidation states. The 2,482 eV map has maximum sensitivity to sulphate (S^{6+}), but also excites the S^{2-} species. Hence, both oxidation states contribute to the total intensity of the sulphur Kα emission line recorded at an excitation energy of 2,482 eV. The amount of this contribution from the S^{2-} species, $I_{S2-,2482eV}$, could be quantified using a known XAS spectrum of the S^{2-} species by calculating $I_{S2-, 2482eV} = \mu I_{S2-,2472eV}$ for the S^{2-} species where μ is the ratio of the intensities at 2,482 and 2,472 eV, as inferred from the XAS spectrum of a pure S^{2-} species. Recorded references (Supporting information) show that μ is on the order of 0.3–0.6, and spectra taken from the sample indicate $\mu < 1$. Therefore, $\mu = 0.5$ is employed, note that the overall results for the distribution of the calculated oxidation states are independent for $0 < \mu < 1$. Based on these considerations, the equations can be formulated to calculate the oxidation state maps:

$$I_{S\ (+VI)} = \left[I_{2482} - \left(I_{2464} + \mu I_{2472} \right) \right] \ eV \tag{1}$$

$$I_{S(-II)} = \left(I_{2472} - I_{2464} \right) \ eV \tag{2}$$

$$I_{tot} = I_{2560} - I_{2464} \ eV \tag{3}$$

This problem has been addressed in the literature in different ways. For example, Perrin et al. (2017) calculated S^{2-} and S^{6+} maps from the equation.

$$I_{(+VI)} = \left(I_{2560} - I_{-2472} \right) \ eV \tag{4}$$

which assumes that only S^{2-} and S^{6+} are present in the samples and that the contribution of the S^{2-} to the sulphur emission line is equal when excited with 2,560 or 2,472 eV. An alternative approach was made by Foriel et al. (2004) who used the value $\mu = 1$ in the equation shown above. This implies that S^{2-} is excited equally at 2,472 and 2,482 eV. Applying both methods finds no practical differences in the estimated relative distributions for S^{6+} and S^{2-} in the samples. If a sufficiently large number of high-quality reference spectra were available, more sulphur species could be determined by employing additional maps taken at different energies, as has been demonstrated by Pickering et al. (2009). This methodology was not followed for two reasons. Most importantly, for complete map speciation fitting, one needs to confirm that the references comprise a complete set of all sulphur species present in the studied system. This is critical, as the method does not involve fitting of full XANES spectra, but rather compares a limited number of data points. As all of the candidate species are not known with sufficient certainty, this analysis was not pursued and the focus was placed on the distribution of the two main oxidation states, S^{2-} and S^{6+}.

In addition to the S^{6+} and S^{2-} distribution maps, the strontium distribution was also derived from the smaller maps (150 μm × 40 μm). For this analysis, a peakfitting (based on the Levenberg–Marquardt algorithm) as implemented in PyMca of the fluorescence spectrum for each individual data point was performed using the PyMca software (Solé et al., 2007). An excitation energy of 2,464 eV, well above the strontium L1 absorption edge (2,216 eV) but below the sulphur K-edge energy, was chosen for this measurement in order to excite all Sr L lines but not the sulphur fluorescence line.

3 | RESULTS AND DISCUSSION

3.1 | Incubation media of *A. islandica* shells

The sterile seawater used for the incubation media contained 2.6 g/l of dissolved sulphate, which is close to concentrations typically observed in marine waters (2.7 g/l), including that of the North Sea. No considerable change in sulphate concentrations during the incubation period was detected in the incubation media and control (anoxic seawater; Table 1).

At the end of the experiments, all experimental media retained their initial sulphate sulphur isotope ratio (Table 1), that is, the sulphur isotope signal of marine sulphate (Johnston et al., 2014), except for the anoxic sediment medium. The anoxic sediment incubation medium yielded a depleted $\delta^{34}S_{SO4}$

value and an elevated $\delta^{18}O_{SO4}$ value compared to both the sterile seawater and the control.

3.2 | Pristine *A. islandica* shells

3.2.1 | Microstructure

Microscopy images of the pristine *A. islandica* shell segment display the typical subdivision of an inner and outer shell layer. Depending on the sampling site along the commissure to hinge transect, the relative proportion of inner to outer shell layer changes (Figures 1–3). The pristine sample is characterised by a thin inner shell layer, implying that it was taken closer to the commissure.

The inner shell part is characterised by a layered structure, whereas the outer shell layer is composed of growth increments which curve towards the outer shell margin (Figures 1A, 2A and 3). The inner shell layer and the regions directly adjacent to the growth lines fluoresce stronger when compared to the rest of the shell (Figure 1B,F; Fichtner et al., 2018). In between the growth lines, growth increments
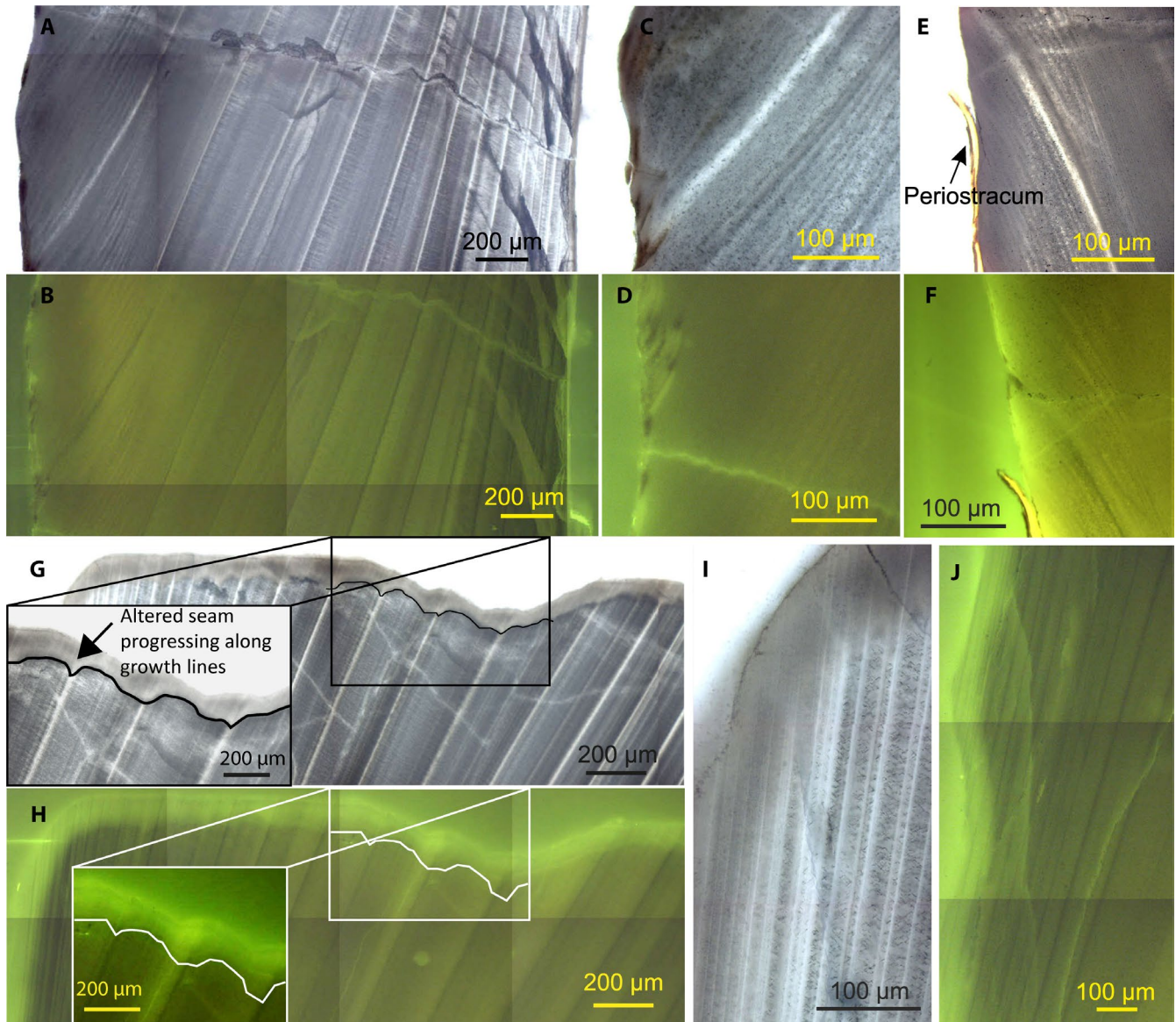
FIGURE 1 Transmitted light (TL) and fluorescence images (FL) of *Arctica islandica* shells. (A–D) Shell incubated in sterile seawater. (A) TL image of shell cross-section. (B) Fluorescence image of shell cross-section. (C) TL image of outer shell margin. (D) FL image of outer shell margin. (E and F) Non-incubated shell. (E) TL image of outer shell margin with periostracum. (F) FL image of the same region. (G–J) Shell incubated in *Shewanella sediminis* culture. (G) TL image shows altered seam around the inner margin and the cut margin. Note, brown margin progresses along the growth lines. (H) FL image of the same region. (I) TL image of the same region. (J) FL image showing extended seam along the whole inner margin. Note, organic-free growth lines are white on TL images, but dark on FL images. Organic-rich lines are dark on TL images and lighter on FL images
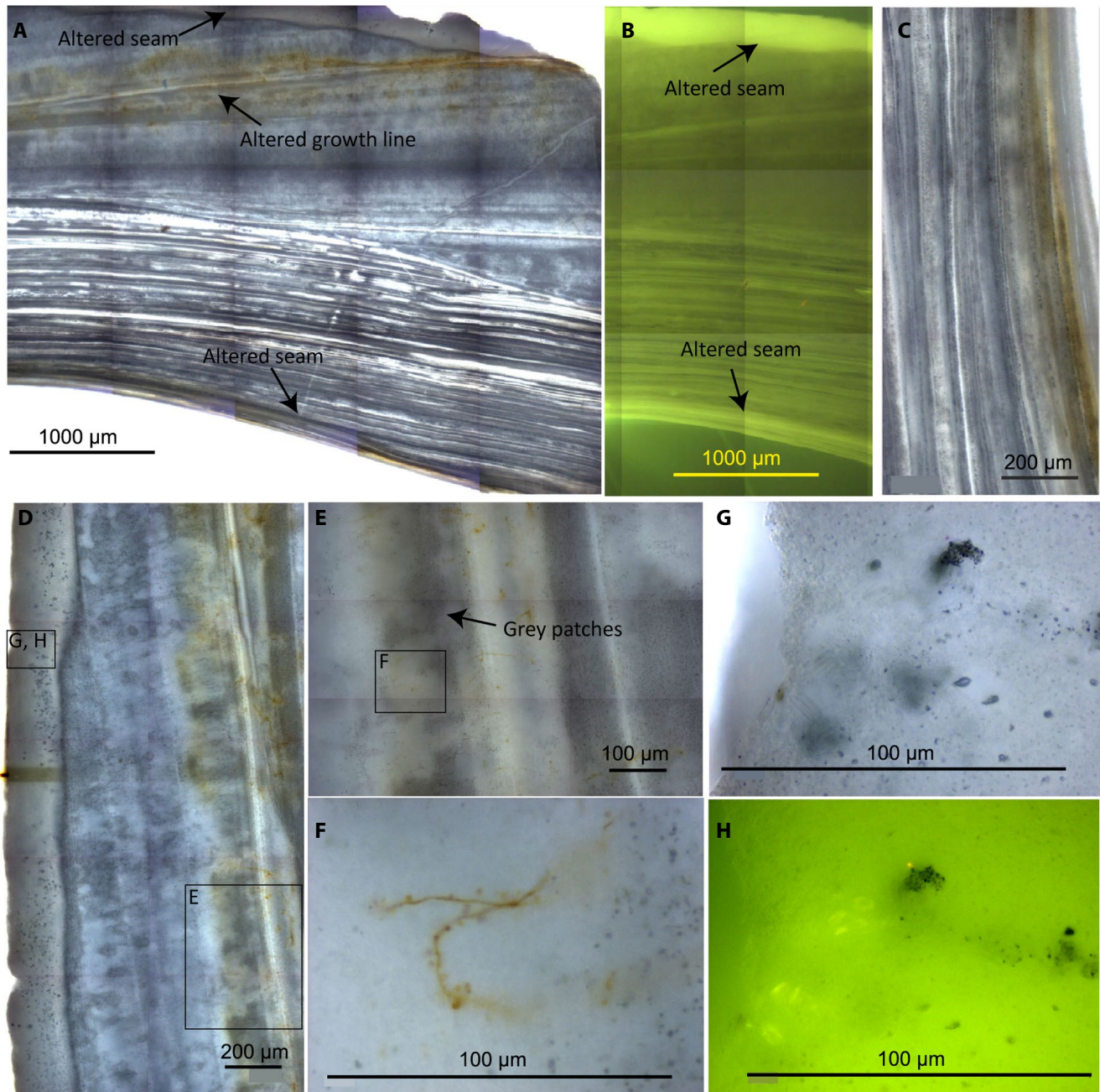
FIGURE 2 Transmitted light (TL) and fluorescence images (FL) of the shell incubated in anoxic sediment slurry. (A) Cross-section overview. The altered seam along the outer shell margin, the altered growth line in the shell center and the different shell structure of the inner shell layer are visible. (B) FL image of the shell cross-section reveals that the altered seam at the outer shell margin and the inner shell margin fluoresces stronger than the other shell parts. (C) TL image of the inner shell margin reveals brown-coloured layers that indicate impact of microbial alteration. (D) TL image of the outer shell margin and the altered growth line. In the center, traces of μ-XRF-mapping are visible. Small black spots in the altered seam, grey patches in the center and brown patches along the white growth line indicate microbial alteration in both the outer and the internal shell regions. (E) TL images of the altered growth line and the grey patches. Darker grey regions display pores as black spots. Light-grey regions are considered altered but contain small brown fibres in lieu of visible pores. (F) TL image of a brown-coloured fibre with visible small red spots along the length. (G) TL image of outer shell margin. Dark accumulations and colourless elongated shapes are visible. (H) FL image of the same region showing stronger fluorescence associated with the elongated shapes

appear as grey intervals with pores containing organic matter (Figure 1). The stronger fluorescence of the inner shell layer as well as of the growth increments of *A. islandica* probably corresponds to locally higher amounts of organic matrices within the shell (Wanamaker et al., 2009). The outer shell margin is covered by the periostracum (Figure 1E).
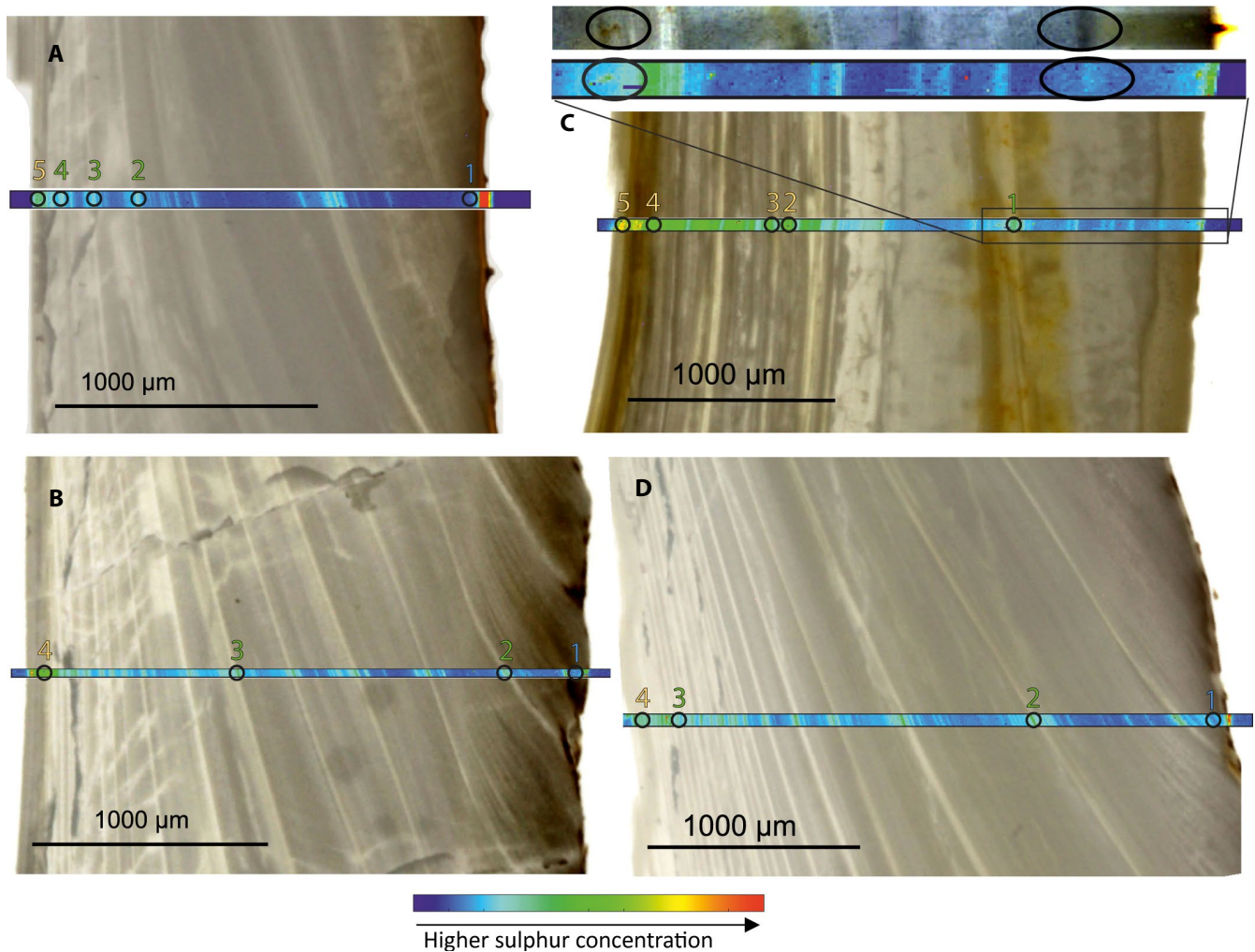
FIGURE 3 Reflected light images of shell thin-sections with sulphur XRF-maps generated at 2,800 eV beam energy. Numbered circles mark points where sulphur XANES spectra were taken (Figure 4). The inner shell layers are on the left, the outer shell layers are on the right side of the images. The colour scale for the sulphur concentration is individual for each sample. (A) Non-incubated shell (previously shown in Fichtner et al., 2018). (B) Shell incubated in sterile seawater. (C) Shell incubated in anoxic sediment slurry with zoom of the areas where largest changes in sulphur distribution and shell colour are observed. (D) Shell incubated in *Shewanella sediminis* culture. Remains of the periostracum are visible at the outer shell margin

3.2.2 | Sulphur isotope composition

Sulphur isotope analyses of CAS and WSS in the pristine *A. islandica* shell revealed a $\delta^{34}S_{CAS}$ value of $+20.6 \pm 0.4‰$ and a $\delta^{34}S_{WSS}$ value of $+17.8 \pm 0.2‰$ (Table 1). To a major extent, sulphate is associated with the mineral part of the shell (as CAS; Dauphin et al., 2003; 2005; Fichtner et al., 2018; Perrin et al., 2017; Tamenori et al., 2014). During CAS incorporation in aragonite, the $\delta^{34}S_{SO4}$ is enriched by $1‰$ (Barkan et al., 2020). The fact that the $\delta^{34}S_{CAS}$ value in the *A. islandica* shell is not $1‰$ higher but instead slightly lower than the primary seawater signal of $21.2‰$ (Johnston et al., 2014) can be explained by a weak vital effect during CAS incorporation, causing slightly depleted values.

In contrast, the lower $\delta^{34}S$ value of the WSS in the *A. islandica* shell is caused by its organic nature and a stronger

vital effect. Organic bonds such as those found in chondroitin sulphate, which is supposed to belong to the WSS fraction, are either being generated or modified during digestive processes within the organism. Another option is that this isotopically lighter sulphate is a result of algae or other microbes entering the bivalve via food uptake. Hence, vital effects during digestion in either the bivalve or in organisms that are digested by the bivalve probably cause isotopic fractionation and a lower $\delta^{34}S$ value of the WSS compared to that of the CAS. However, the exact process of CAS and WSS incorporation into bivalve shells and how the pathways differ from each other, is still not thoroughly understood.

The acid-insoluble organic matter comprises the reduced sulphur phases of the *A. islandica* shell (Fichtner et al., 2018) and has a $\delta^{34}S$ value of $+10.7 \pm 0.4‰$ (Table 1). These sulphur phases can be present in material that is filtered from
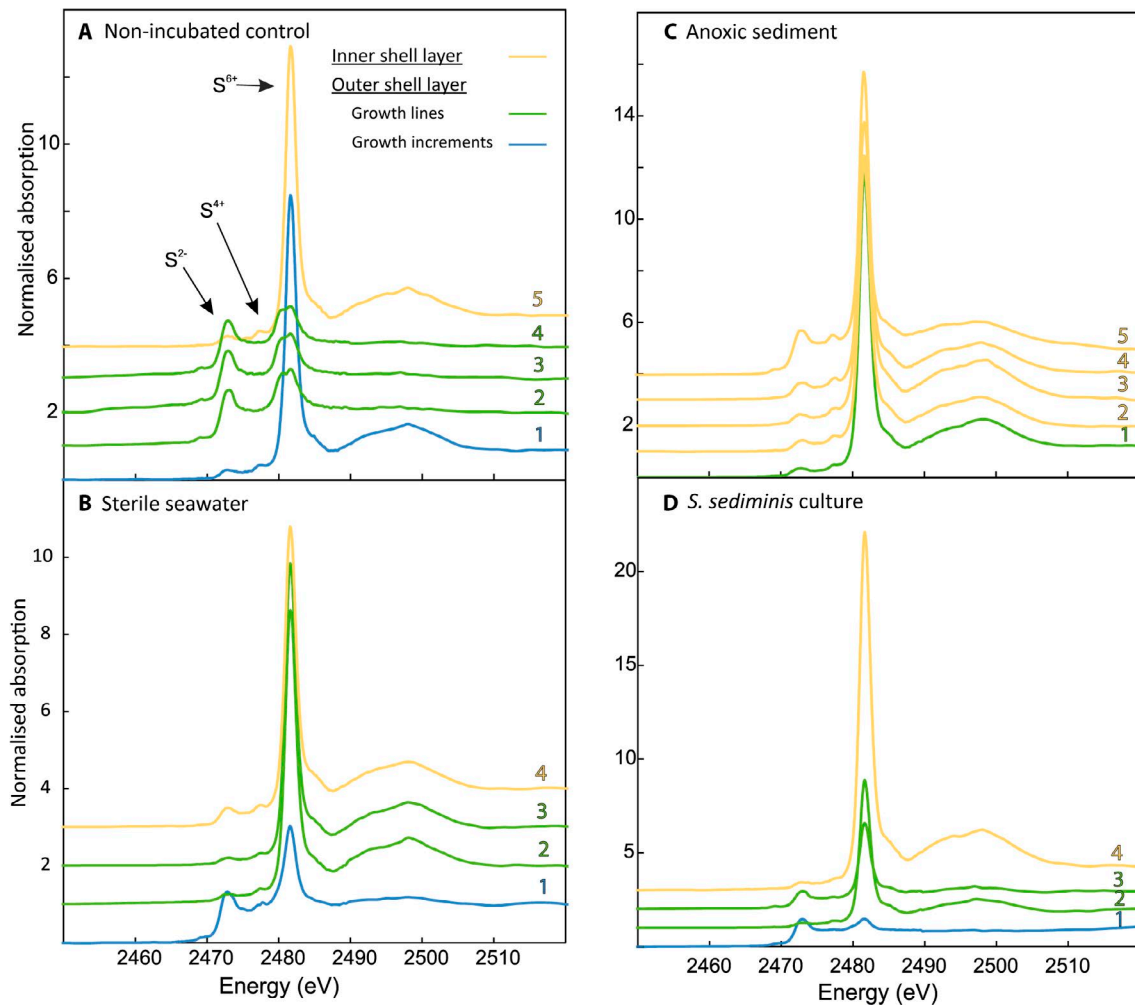
FIGURE 4 Sulphur XANES spectra of *Arctica islandica* shell segments. Numbers indicate the positions where the spectra were taken (see Figure 3). (A) Non-incubated sample. (B) Sample incubated in sterile seawater. (C) Sample incubated in anoxic sediment slurry. (D) Sample incubated in *Shewanella sediminis* culture

the seawater by the organism. In the marine environment, several algae and bacteria conduct assimilatory sulphate reduction to generate certain organic phases, such as sulphur-bearing amino acids (Peck & Lissolo, 1988; Schiff & Fankhauser, 1981). Assimilatory sulphate reduction causes a sulphur isotopic fractionation which is less pronounced than the fractionation that occurs during dissimilatory sulphate reduction (Kaplan & Rittenberg, 1964). During food uptake via filtration the reduced sulphur phases can enter the organism and be subsequently incorporated into the intra-shell organic matter. To what extent these reduced sulphur phases undergo additional isotopic fractionation during digestion remains unknown.

3.2.3 | Sulphur XANES spectra

Sulphur XANES spectra of the *A. islandica* samples were measured in situ along a cross-section from the inner to the outer shell rim (Figure 3). The spectra show that sulphur in the shell is present in various inorganic and organic forms. Within the bivalve shell, there is a clear dominance of S^{6+} as indicated by peaks at 2,482 eV. This oxidised sulphur can be bound as chondroitin sulphate or substituting for the carbonate ion in the crystal lattice as CAS. A comparison with the different sulphate mineral reference spectra (Supporting information) excludes the presence of a particular sulphate mineral within the shell. The split in the sulphate peak observed in spectra 2, 3 and 4 of Figure 4A is most likely a mixture between an amorphous and a crystalline component. Perrin et al. (2017) reported an enlarged sulphate peak (at 2,482.7 eV) taken on dried polyp tissue from a coral skeleton and explained this as a presence of S^{5+}, probably caused by sulphonate in L-cysteic acid. Alternatively, Richardson et al. (2019) suggested that a shoulder on the low-energy side of the sulphate peak is due to a sulphate ester. Hence, in the case of the *A. islandica* shell, it is possible that small amounts of a sulphonate group or a sulphate ester could have caused the
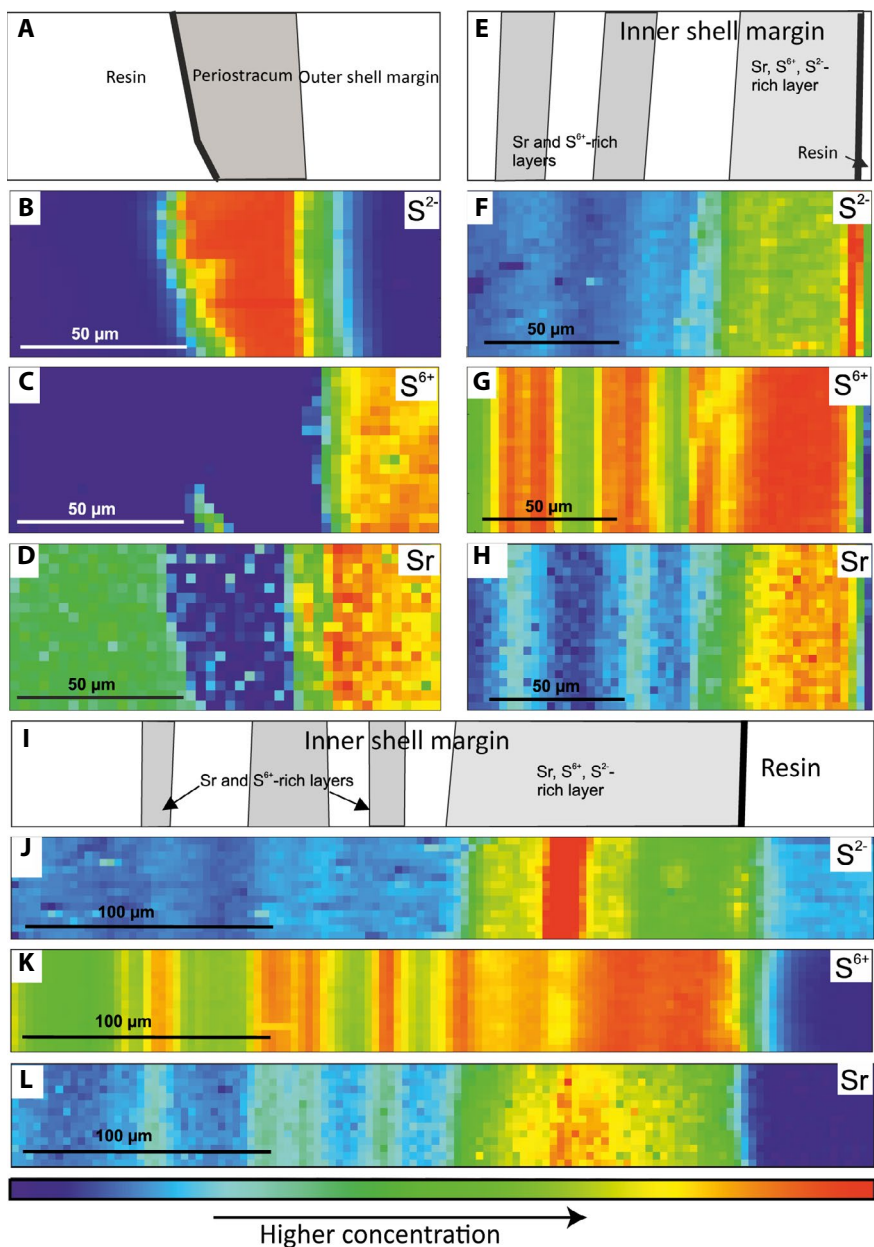
FIGURE 5 S^{2-}, S^{6+} and Sr distribution patterns along *Arctica islandica* shell margins of control samples. Concentrations are displayed on individual scales. (A–D) Periostracum of the non-incubated shell. (A) Sketch map. Distribution pattern of (B) S^{2-} (C) S^{6+}. (D) Sr. (E–H) Inner shell layer of the non-incubated shell. (E) Sketch map. Distribution pattern of (F) S^{2-} (G) S^{6+} (H) Sr. (I–L) Inner shell layer of shell incubated in sterile seawater medium. (I) Sketch map. Distribution pattern of (J) S^{2-}. K: S^{6+}. (L) Sr. Note that the strontium maps were processed with PYMCA, but the S^{6+} and S^{2-} maps were calculated from raw data

split in the sulphate peak. A minor presence of sulphite (S^{4+}) is indicated by small peaks at 2,477 eV. Similar to sulphate, sulphite is considered to substitute for the carbonate ion in the aragonite shell. There is also a clear occurrence of S^{2-} as indicated by peaks at 2,472 eV (Figure 4), which can be attributed to the presence of amino acids such as L-methionine, L-cystine, or to glutathione (Supporting information, Perrin et al., 2017).

Comparison between the pristine sample and the control sample incubated in sterile seawater reveals different proportions of the various sulphur species in the inner shell layer, the growth lines and the growth increments. The inner shell layer seems to be dominated by S^{6+} compared to S^{2-} in both the non-incubated and the control sample. However, the sulphur speciation maps revealed that S^{2-} can be enriched in certain portions of the inner shell layer (Figure 5F,K). The

growth lines of the pristine sample reveal a clear presence of S^{2-} and minor presence of S^{6+}, which was not observed in the growth lines of the control sample, where the XANES spectra showed a clear dominance of S^{6+} and almost no S^{2-} (Figure 4B, spectra 2, 3). An oxidation of S^{2-} in those central growth lines is unlikely to happen because of the anoxic incubation conditions, and because the inner shell margin is still rich in S^{2-} (Figure 5J) and seems to be unaltered. Additionally, the XANES spectrum taken on a growth increment of the control sample shows a higher proportion of S^{2-} than that of the pristine sample. Thus, from the XANES spectra alone, a characteristic proportion of reduced and oxidised sulphur species cannot be attributed to each of the three locations. Therefore, it is necessary to consider the relative abundance of reduced and oxidised sulphur phases in the growth lines and growth increments of both the pristine and the control
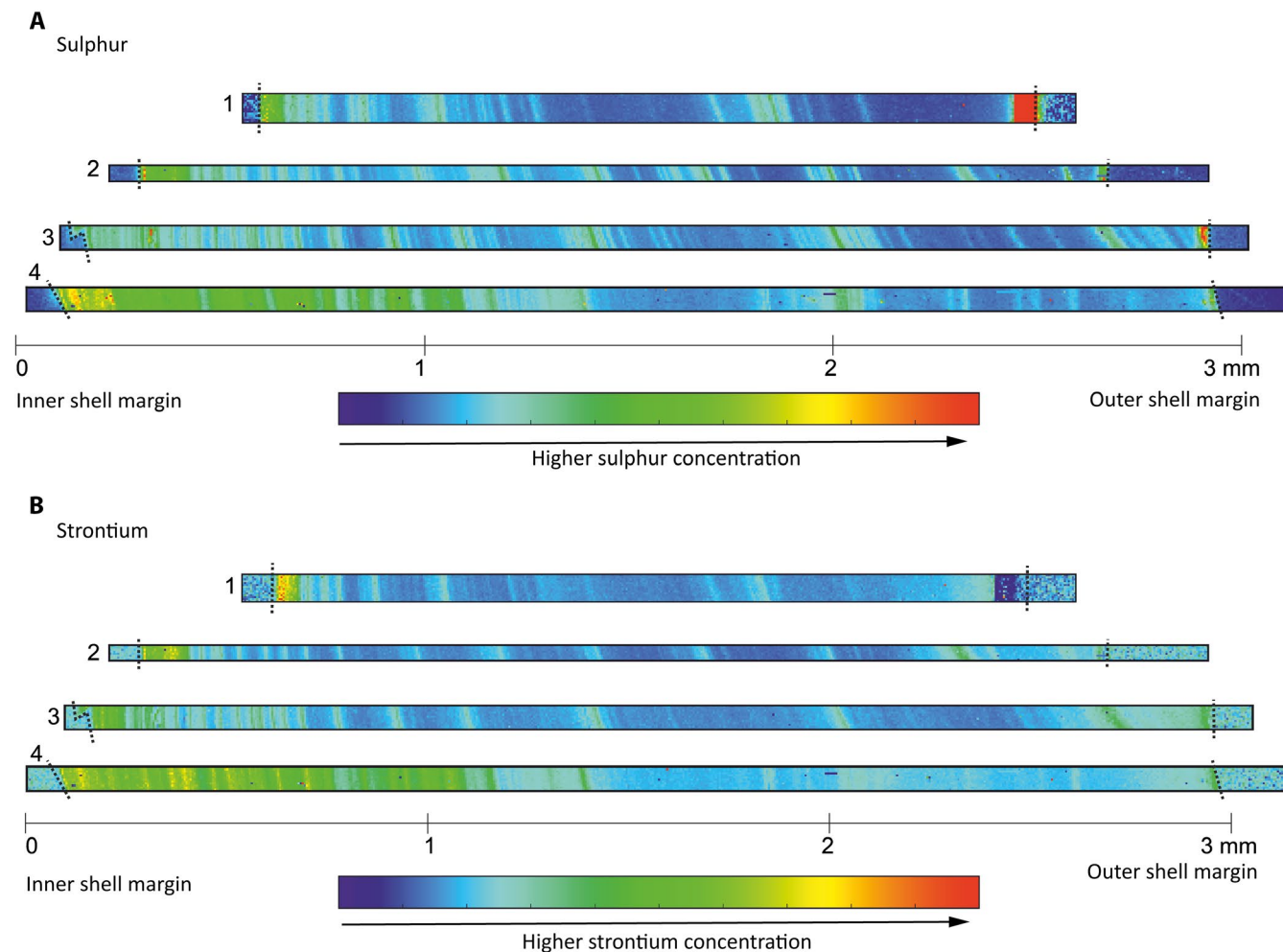
FIGURE 6 Sulphur (A) and strontium (B) μ-XRF maps along cross-sections of *Arctica islandica* shells. The inner shell layer is on the left side, and the outer shell layer is on the right side of the map. Dashed lines indicate the resin boundary. Maps of different samples are displayed using the same colour scale, but different for sulphur and strontium. 1: Non-incubated shell. 2: Shell incubated in sterile seawater medium. 3: Shell incubated in S*hewanella sediminis* culture. 4: Shell incubated in anoxic sediment slurry. Strontium maps of 1, 3 and 4 were previously published by Lange et al. (2018). Sulphur and strontium map of the non-incubated shell was previously published by Fichtner et al. (2018). The inner shell layer as well as annual growth lines are characterised by enriched sulphur and strontium concentrations. The periostracum present in 1 and 4 is enriched in sulphur, but devoid of strontium

samples as showing natural heterogeneity of the non-altered shell.

3.2.4 | Sulphur and strontium μ-XRF mapping

The sulphur and strontium distribution patterns reflect the subdivision of an inner and an outer shell layer, and an outer periostracum. The maximum sulphur presence was observed in the periostracum, the protective organic layer on the outer shell. It shows a clear dominance of S^{2-} and the absence of S^{6+} and strontium (Figure 5B–D).

A comparably high sulphur proportion was observed in the inner shell layer, especially at the inner shell rim (Figures 3 and 6; Fichtner et al., 2018). Maps of sulphur oxidation states along the pristine inner shell margin reveal a layered distribution of S^{6+} and S^{2-} (Figure 5E through L). S^{6+} is enriched along the inner shell margin and shows a positive correlation with strontium. Because strontium is exclusively present in the inorganic components of the shell, the positive correlation indicates that S^{6+} is primarily inorganic in nature and structurally substituted in the carbonate (Perrin et al., 2017). S^{2-} is strongly enriched in the outermost portions of the pristine inner shell margin (Figure 5F,K).

In the outer shell layer, sulphur is present along the annual (and possibly sub-annual) growth lines (Figures 3 and 6). Strontium concentrations are also higher along the growth lines (Figure 6B). This positive correlation between sulphur and strontium indicates that the sulphur along the growth lines is inorganically bound, presumably as sulphate. However, XANES spectra (Figures 3 and 4A) reveal

that reduced sulphur species are also present in these areas. Therefore, the higher sulphur abundance along the growth lines can be attributed to higher amounts of sulphur content both the mineral and the organic components.

3.3 | *Arctica islandica* shells incubated in *S. sediminis* medium

Results shown here reveal no alteration of the $\delta^{34}S_{CAS}$ value. Instead, the data reveal the degradation of intra-shell organic matter in *A. islandica* shells that can be interpreted as the result of the 3 month incubation in the *S. sediminis* culture. Microscopic images of the altered *A. islandica* subsample indicate modified organic content evidenced by surficial brown staining progressing along organic-rich areas adjacent to the growth lines (*ca* 80 µm thick) from the margin to the shell center (Figure 1G). Bright green fluorescence images of these areas confirm this modification of the type and distribution of organic matter (compare Figure 1G,H). The presence of *S. sediminis* could not be detected with fluorescence because the bacterium is not auto-fluorescent at the used excitation wavelength (Zhao et al., 2005). However, decreased Ca concentrations in the outer shell regions relative to the inner shell parts (from 39 wt% at the beginning to 31% after the incubation) and dissolution features detected via SEM imaging indicate partial dissolution caused by the oxidation of chitin, and subsequent fermentation of chitin monomers by *S. sediminis* (figure 6 in Lange et al., 2018). The acidic fermentation products not only led to partial shell dissolution, but probably also caused the discolouration of the shell near the oxidised organic matter (Figure 1G,I).

Elemental maps covering the whole shell transect are characterised by sulphur and strontium distributions similar to the pristine shell (Figure 6). Differences in the sulphur and strontium distribution correlate with microstructure, the shape and number of growth lines, or the thickness of the inner shell layer. A modified distribution along the stained seam as reported for the calcium distribution in Lange et al. (2018) was not observed. Due to the small change in calcium concentrations, possible small variations in strontium and mineral-bound sulphate are probably not detectable. The concentration and the $\delta^{34}S$ value of the dissolved sulphate in the medium (Table 1) as well as the $\delta^{34}S_{CAS}$ (+20.8 ± 0.0‰) value in the shell remained unaffected by the degradation process at this stage. However, it is proposed that with progressive dissolution of the metastable aragonitic shell material and related organics, CAS would be liberated into the fluid.

The lower $\delta^{34}S_{WSS}$ value of +12.7 ± 0.4‰ compared to +17.8 ± 0.2‰ in the pristine sample (Table 1; Fichtner et al., 2018) is considered clear evidence for modified organic matter. In the pristine *A. islandica* shell, WSS represents the sulphate fraction of the soluble organic matter, such as chondroitin sulphate (Fichtner et al., 2018). One reason for this deviation in $\delta^{34}S_{WSS}$ is the influence of the acid-insoluble organic matter which has a lower $\delta^{34}S$ value of +10.7 ± 0.4‰ (Table 1). Thus, it seems likely that this insoluble organic matter was bacterially degraded and the reduced sulphur (S^{2-}) was oxidised, as in addition to the ability to ferment the chitin monomer N-acetylglucosamine, *S. sediminis* also metabolises other sulphur-bearing amino acids and sugars (Zhao et al., 2005). The XANES spectrum taken along the inner shell margin (#4 in Figure 4D) reveals relatively lower amounts of S^{2-} compared to the non-incubated and control
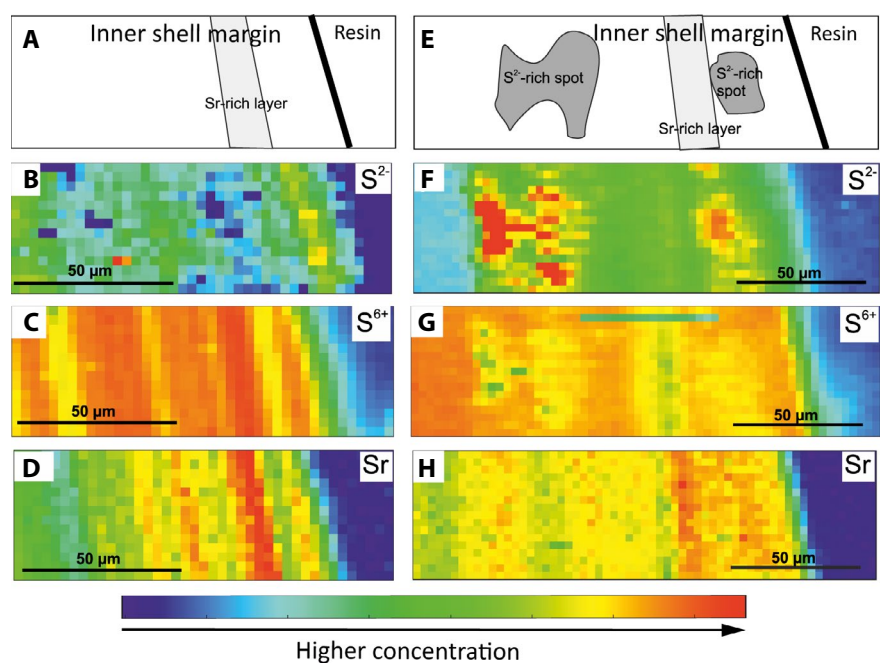
FIGURE 7 S^{2-}, S^{6+} and Sr distribution patterns along inner margins of microbially altered *Arctica islandica* shell samples. Concentrations are displayed on individual scales. (A–D) Shell incubated in *Shewanella sediminis* culture. (A) Sketch map. Distribution pattern of (B) S^{2-} (C) S^{6+}. (D) Sr. (E–H) Shell incubated in anoxic sediment slurry. (E) Sketch map. Distribution pattern of (F) S^{2-} (G) S^{6+} (H) Sr. Note, the strontium maps were processed with PYMCA, but the S^{6+} and S^{2-} maps were calculated from raw data

samples (Figure 4A,B). Additionally, the primarily layered S^{2-} distribution changed to patchy distribution (Figure 7B), while the sulphate (S^{6+}) retained its original layered pattern (Figure 7C). These results confirm the degradation of insoluble organic matter and suggest an oxidation of S^{2-} leading to a lower $\delta^{34}S$ value in the WSS.

3.4 | *Arctica islandica* shells incubated in an anoxic sediment slurry

3.4.1 | Alteration of shell microstructure and sulphur phases in the shell

The sample incubated in the anoxic sediment slurry exhibits multiple alteration features, including stronger fluorescence compared to the non-altered sample and discoloured outer shell margins (Figure 2B) with slightly higher sulphur proportions than the central shell region (Figure 3C). As the altered interval is restricted to the shell rim and contains fluorescent spots (Figure 2H), these alteration features are probably the consequence of microbial activity.

The brownish staining as well as the patchy distribution of reduced sulphur (S^{2-}) on the organic-rich inner shell layer indicates microbial alteration (Figure 7F). Black patches (*ca* 20 μm) are visible in the inner shell margin and consist of clusters of dark-green spots (<1 μm in diameter) (Figure 2D,G). Adjacent to these accumulations, at the outermost shell margin, elongated colourless zones occur with a stronger fluorescence relative to the host shell (Figure 2G,H). The inner shell margin is partly brown in colour (Figure 2C). Microscopy images exhibit a prominent slightly brown growth line (Figure 2A,C,D) along which thin rust-coloured fibres are connected to red spots (*ca* 1 μm; Figure 2F). These spots were not characterised further, but the modification of the microstructure along the growth line is in agreement with the development of small zones of increased sulphur abundance relative to the surrounding areas (Figure 3C). Reduced sulphur species and organic matter are enriched directly adjacent to the growth lines of pristine *A. islandica* shells (Fichtner et al., 2018; Schöne et al., 2011). Thus, the higher sulphur concentrations (Figure 3C) suggest microbial consumption of sulphur-bearing organic material. The XANES spectrum taken on the growth line primarily reflects oxidised sulphur from the mineral phase and does not indicate modification of organic matter in that area (Figure 4C, spectrum 1).

However, from the central part (Figure 4C, spectrum 2) to the inner shell rim (spectrum 5), the relative proportion of S^{2-} increases. The S^{2-} peak at 2,472 eV of spectrum 7 of the incubated shell sample (Figure 4C) is much more pronounced than the S^{2-} peaks of the spectra from the inner shell rims of the non-incubated sample (Figure 4A, spectrum 5),

the sample incubated in sterile seawater (Figure 4B, spectrum 4), and the sample incubated in the *S. sediminis* culture (Figure 4D, spectrum 4). This slight enrichment in S^{2-} in the altered shell implies reduction of existing sulphate phases. This is confirmed by the sulphur speciation maps, which reveal a patchy S^{2-} distribution along the inner shell margin with maximum abundance at locations of minimum S^{6+} abundance (Figure 7F,G). This supports the idea of sulphate reduction and local enrichment of reduced sulphur phases.

In contrast to the local enrichment of S^{2-} along the inner shell margin, the $\delta^{34}S_{WSS}$ value of the bulk sample indicates oxidation of reduced organic sulphur: The relatively lower $\delta^{34}S_{WSS}$ value of +14.6‰ compared to +17.8‰ in the pristine bivalve shell (Table 1) is evidence for modification of the soluble sulphate. This lower $\delta^{34}S_{WSS}$ value is comparable to the sample incubated in the *S. sediminis* medium, where the low $\delta^{34}S_{WSS}$ value may be explained by the oxidation of reduced sulphur phases during degradation of the isotopically light insoluble organic matter (see Section 3.3). Accordingly, the *S. sediminis* sample had no indication of S^{2-} species enrichment but rather for depletion. In contrast, the sample incubated in the multi-microbial anoxic sediment slurry shows an enrichment of reduced sulphur phases. One explanation for the low $\delta^{34}S_{WSS}$ value is that the anoxic sediment contains a variety of different microbes, probably including *S. sediminis*. Therefore, the formation of reduced sulphur species in the inner shell margin can be caused by sulphate reducing microbes, while the isotopic signal of the WSS can be a result of metabolisms of other microbes that oxidise reduced organic sulphur compounds.

The $\delta^{34}S_{CAS}$ value in the incubated shell sample is slightly enriched (+21.9 ± 0.5‰) compared to the $\delta^{34}S_{CAS}$ value in the pristine shells (+21.0‰ ± 0.1; 20.6‰ ± 0.4). A change in $\delta^{34}S_{CAS}$ implies incorporation from aqueous sulphate from the medium into the shell. Three scenarios are discussed to explain how this may have happened:

1. The shell experienced a preferential loss of low $\delta^{34}S_{CAS}$ values, and the $\delta^{34}S_{CAS}$ moved towards equilibrium with the $\delta^{34}S_{SO4}$ of the incubation medium. Barkan et al. (2020) reported an isotopic enrichment of 1‰ for $\delta^{34}S_{CAS}$ in aragonite compared to aqueous sulphate. However, because of the ongoing organic processes in and around the shell, it is purely speculative to what extent an equilibrium between aragonitic shell and medium could develop.

2. In the anoxic sediment microbial sulphate reduction (MSR) occurred, which led to a ^{34}S-enrichment in the aqueous sulphate. This isotopically enriched sulphate could have been incorporated in the aragonite shell, increasing the $\delta^{34}S_{CAS}$. However, the dissolved sulphate in the incubation medium revealed a lower $\delta^{34}S$ value (+18.3‰) compared to the sterilised seawater (+20.5‰) and the control

medium (20.4‰). Thus, it seems unlikely that MSR in the slurry caused the enrichment in $\delta^{34}S_{CAS}$ (see 3.4.2 for discussion of the $\delta^{34}S$ of the aqueous sulphate).

3. Microbial sulphate reduction occurred in the inner shell layer and led to an increased $\delta^{34}S_{CAS}$ value. Sulphur speciation maps and XANES spectra revealed a local enrichment of reduced sulphur species along the inner shell margin. A limited exchange between intra-shell fluids and the incubation medium would have been necessary to reach a sufficient enrichment in ^{34}S of the dissolved intra-shell sulphate. During subsequent dissolution and recrystallisation of the aragonite, this sulphate could have been incorporated into the shell.

Ultimately, any alteration of CAS requires dissolution and re-precipitation of the host carbonate. However, although dissolution features along the segment surfaces were observed via SEM (Lange et al., 2018), no indications of re-precipitation, for example altered $\delta^{13}C_{CARB}$ or $\delta^{18}O_{CARB}$ values or the presence of newly formed calcite (detectable via Raman spectroscopy) were found (Lange et al., 2018). Furthermore, the preservation of primary strontium distribution patterns (higher abundance along the growth lines and inner shell margin and lower abundance in the growth increments) along the microbially altered growth line indicated negligible aragonite dissolution (Figures 3C and 6B-4). Therefore, it remains unclear what caused the slightly enriched $\delta^{34}S_{CAS}$ value in the sample incubated in the anoxic sediment slurry.

3.4.2 | Dissolved sulphate in the incubation medium

The slightly more ^{32}S-enriched isotopic composition of dissolved sulphate in the anoxic incubation medium (+20.5 ± 0.08‰ vs +18.3 ± 0.04‰; Table 1) may be a result of microbial consumption of S^{2-}-bearing intra-shell organic matter. However, as the sulphate concentration in the incubation medium was not considerably affected (Table 1), the intra-shell organic matter can be refuted as the main source for the lower $\delta^{34}S$ value of the dissolved sulphate. It rather requires a contribution from an isotopically light sulphur phase with a $\delta^{34}S$ value of −40‰ or less. Assuming MSR and formation of H_2S occurred within the anoxic medium containing natural microbial communities, it is possible that a pre-existing sulphide phase within the natural anoxic sediment slurry oxidised during the duration of the incubation. As indicated by the higher $\delta^{18}O$ value (+7.7 ± 0.2‰ prior to incubation versus +10.0 ± 0.2‰ after incubation) of the dissolved sulphate, air contamination might have caused the oxidation of dissolved H_2S in the anoxic incubation medium. Although an interruption in
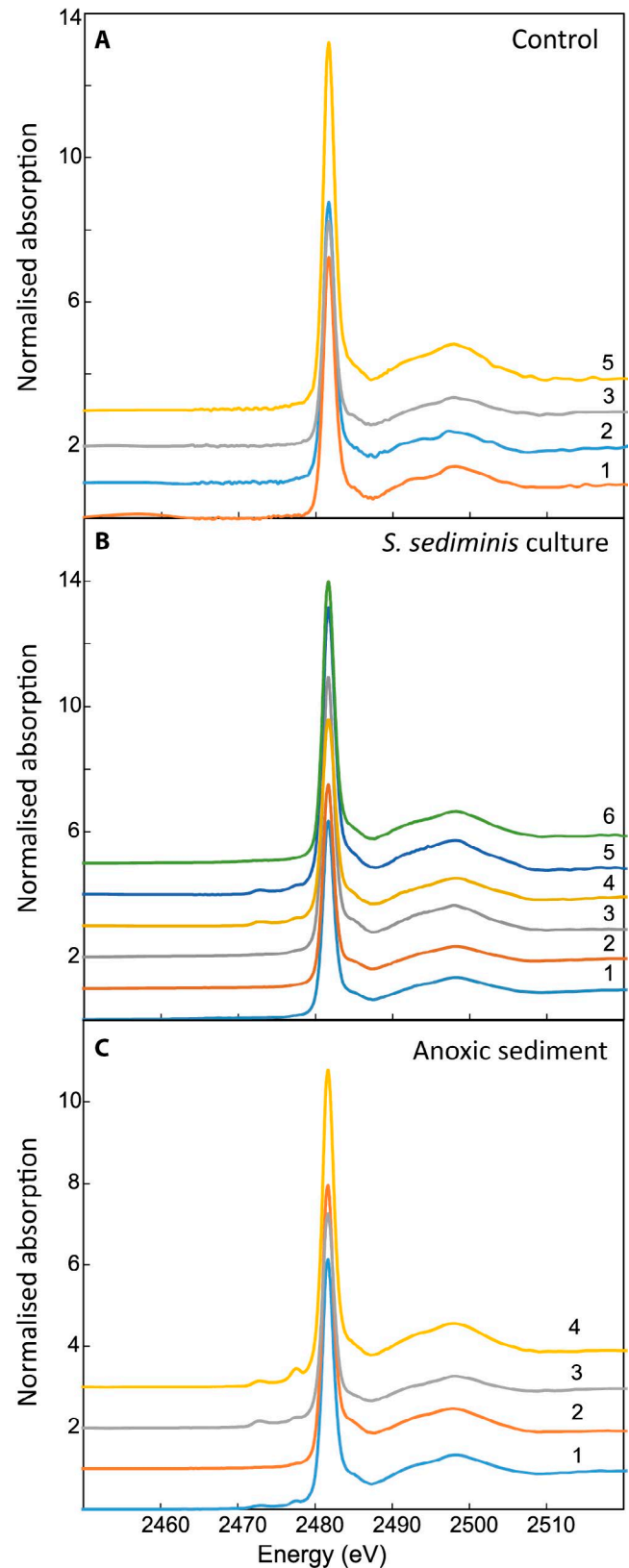
FIGURE 8 Sulphur XANES spectra of *Porites* sp. segments. Numbers indicate the positions where the spectra were taken (see Figure 9). (A) Non-incubated sample. (B) Sample incubated in S*hewanella sediminis* culture. (C) Sample incubated in anoxic sediment slurry
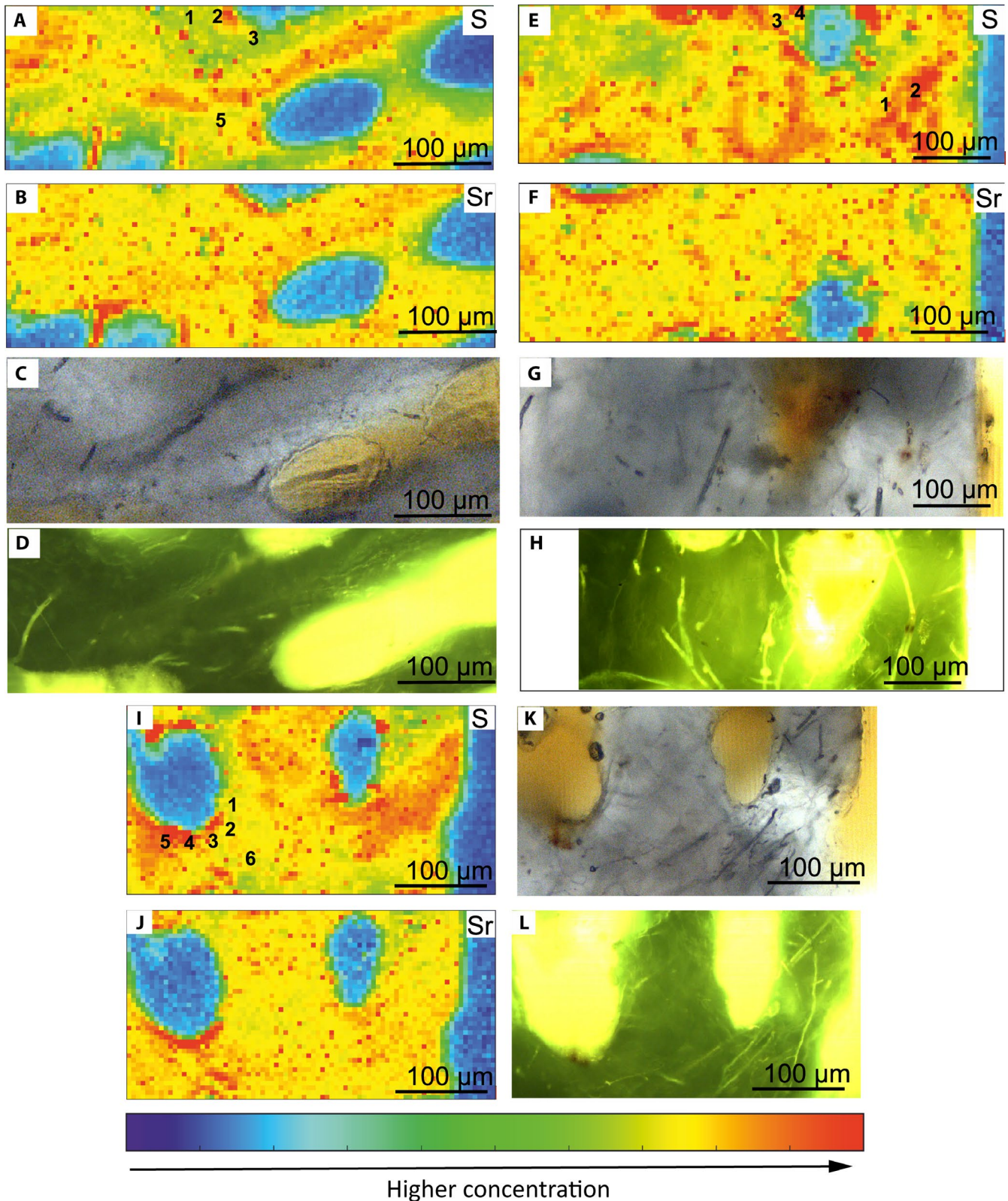
FIGURE 9 FMicro-XRF maps of sulphur and strontium, transmitted light (TL) and fluorescence light (FL) images of the *Porites* sp. segments generated with a beam energy of 2,600 eV. Data were fitted with PYMCA. Numbers on the sulphur maps indicate locations where the XANES spectra were taken (Figure 8). (A–D) Control segment. (A) Sulphur distribution and (B) Strontium distribution of the control segment. (C) TL and (D) FL images of the same segment. (E–H) Segment incubated in anoxic sediment slurry. (E) Sulphur distribution and (F) Strontium distribution of the segment incubated in anoxic sediment slurry. (G) TL and (H) FL images of the same segment. (I–L) Segments incubated in *Shewanella sediminis* culture. (I) Sulphur distribution and (J) Strontium distribution of the segment incubated in *S. sediminis* culture. (K) TL and (L) FL images of the same segment. Note, the strong fluorescence in the coral pores and the brown colour observed on the TL images is due to the resin and not controlled by the coral skeleton

the anoxic conditions during the duration of the experiment was excluded (Lange et al., 2018) by the added resazurin/ resorufin indicator, oxygen contamination during post-experimental analysis and precipitation of aqueous sulphate cannot be ruled out (see Section 2.4). Another process that causes ^{18}O-enrichment in dissolved sulphate is microbial disproportionation of elemental sulphur to sulphide and sulphate (Böttcher et al., 2001), which is common in near-surface sediments (Thamdrup et al., 1993). However, since it has also been found to enrich the δ^{34}S ratio of dissolved sulphate (Böttcher et al., 2001), it remains unclear if (and to what extent) microbial sulphur disproportionation caused the enriched δ^{18}O$_{SO4}$ values. Thus, the lower δ^{34}S value of the dissolved sulphate in the incubation medium cannot be directly attributed to microbial activity during incubation of the *A. islandica* shell.

3.5 | Sulphur in *Porites* sp. skeleton

Sulphur in the coral skeletons is almost entirely attributed to sulphate (Figure 8), with only traces of S^{4+} and S^{2-} species. (Figure 8B,C). Yet, the coral segment incubated in the *S. sediminis* culture exhibited minor amounts of S^{4+} and S^{2-} along the pore rims at sulphur-rich regions (Figure 9). The XANES spectra taken in the more central areas of the skeleton indicated a dominance of sulphate. The XANES spectra of the sample altered in the anoxic sediment slurry reveal a minor presence of S^{2-} and slightly more S^{4+} along the pore margins (Figure 9), which correlate with higher sulphur abundance.

Coral samples incubated in the *S. sediminis* culture reveal sulphur enrichment at pore margins. Increased sulphur concentrations show correlations with minor amounts of S^{2-} and S^{4+} (identified via XANES spectra; Figure 8B). Micro-XRF images suggest an inherent variability of sulphur distribution within the samples, as no changes were detected in the mineral microstructure (Figure 9). Thus, the sulphur-rich areas along the pore margins may represent a biomineralisation characteristic, with initially higher amounts of organically bound sulphur.

3.6 | Comparison of the alteration patterns between *A. islandica* shell and *Porites* sp. skeleton and implications for biogenic carbonates as archives for past seawater properties

Microbial incubation of *A. islandica* shell segments resulted in an alteration of the shell microstructure, organic matter and sulphur species along the shell surface and organic-rich zones in the shell interior. In contrast, the studied coral samples lack comparable alteration features. This is remarkable

due to the inherently higher porosity and permeability and resultant higher surface area available for colonisation by microbes in coral aragonite compared to the bivalve shell. A possible reason for this might be the initially lower organic content in the coral skeleton ultrastructure compared to the bivalve shell as suggested by a weaker fluorescence (Figures 1 and 9; Pederson et al., 2020; Wanamaker et al., 2009) and by different C_{org} values that are 0.35% for the bivalve bulk aragonite and 0.04% for the coral (Lange, 2017). This observation is consistent with results from Glover and Kidwell (1993) who reported more intense microbial degradation in organic-rich shells compared to organic-lean ones.

A principal difference between the incorporation of organic components in bivalves and scleractinian corals was reported in previous studies (Lowenstam & Weiner, 1989; Weiner, 1984), and is reflected in the proportion of S^{2-} and S^{6+} phases in the *Porites* and *A. islandica* samples. Sulphur K XANES spectra of the *Porites* samples show sulphur occurring almost exclusively as inorganic sulphate (Figure 8). Other coral species also contain S^{6+} as the dominant sulphur species, which was attributed to the mineral phase (Nguyen et al., 2014; Perrin et al., 2017; Pingitore et al., 1995; Tamenori et al., 2014). However, in *A. islandica* reduced sulphur was observed exclusively in the insoluble organic matter of the shell (Fichtner et al., 2018). Thus, the near absence of reduced sulphur species in the coral may indicate a comparatively lower organic content in the coral compared to the bivalve shell.

The sulphur isotope values in the organic portion of the *A. islandica* shell are capable of reflecting the subtle effects of the earliest microbial alteration. Other proxy data such as δ^{34}S$_{CAS}$, δ^{18}O$_{CARB}$ or δ^{13}C$_{CARB}$ values are insensitive to this earliest stage of alteration (Lange et al., 2018). Sejrup and Haugen (1994) discussed the microbial consumption of amino acids along the growth lines of recent to early Pleistocene specimens of *A. islandica*, and found that differences in the degree of degradation primarily depended on the duration of exposure to a microbe-rich environment during early diagenesis. This is in accordance with the present results from both incubation media, which indicated oxidation of reduced sulphur in insoluble organic matter, including amino acids. Hence, in the case of the *A. islandica* shell, the microbial consumption of amino acids in intra-shell organic tissue could be diagnostic of earliest marine diagenesis. The extent of applicability of this to other biogenic carbonates, however, is dependent on the amino acid content in the respective carbonate and should be investigated for additional marine calcifying species as well as locations.

4 | CONCLUSIONS

Incubation experiments conducted in this study document the effects of anaerobic microbial activity on biogenic

aragonite with a specific focus on sulphur. Results shown here indicate that CAS was not significantly affected during the incubation. This is consistent with observations of Lange et al. (2018) who reported dissolution features on the incubated samples but did not observe any indications for newly precipitated carbonate. However, microbial alteration degraded intra-shell organic matter within the 3-month incubation period. The extent and the type of alteration was controlled by the different microbial species and communities that surrounded and entered the carbonate. Shell segments of *A. islandica* display alteration of intra-shell organic-rich locations as well as a modified $\delta^{34}S$ value of the soluble organic matter (extracted as WSS) compared to the pristine shell sample. Incubation in an *S. sediminis* medium resulted in decreased S^{2-} concentrations within the shell, whereas incubation in the natural anoxic medium led to higher S^{2-} concentrations along the inner shell margin and a modified sulphur distribution in an organic-rich central region of the shell. The fact that the highly porous nature of the *Porites* sp. coral skeleton resulted in minor-to-no alteration features when exposed to the same conditions can be explained by the relatively low organic content compared to the bivalve shell. The different reduced sulphur concentrations in the bivalve shell and coral skeleton reflect the variation in concentrations of organic matter. This notion emphasises the importance of (bio)mineral—organic matter patterns in carbonate diagenesis and archive preservation. Here, the conclusion is that the concentration of organic matter rather than the pore volume is the controlling factor for the intensity of microbial alteration.

Skeletal material that is naturally exposed *post mortem* to microbe–biomineral interaction for several months is often considered pristine and hence, suitable for palaeoenvironmental reconstruction. This notion might be simplistic based on the data shown here. The present study shows how microbial degradation of S^{2-}-bearing intra-shell organics can modify the $\delta^{34}S_{WSS}$ in biogenic aragonite over extremely short geological time scales, given sufficient primary intra-shell organic matter. The decomposition of the protecting intra-shell organic matter is a prerequisite for alteration of the biogenic carbonate including geochemical seawater proxies such as CAS. The interaction between microbes and organic matter in biogenic hardparts merits consideration in carbonate archive research.

ACKNOWLEDGEMENTS

CONFLICT OF INTEREST

The authors have no conflict of interest to declare.

DATA AVAILABILITY STATEMENT

The data for this study are shown in the various figures and in the table.

ORCID

Vanessa Fichtner https://orcid.org/0000-0002-9470-357X

REFERENCES

Barkan, Y., Paris, G., Webb, S.M., Adkins, J.F. & Halevy, I. (2020) Sulfur isotope fractionation between aqueous and carbonate-associated sulfate in abiotic calcite and aragonite. *Geochimica et Cosmochimica Acta*, *280*, 317–339. https://doi.org/10.1016/j.gca.2020.03.022

Böttcher, M.E., Thamdrup, B.O. & Vennemann, T.W. (2001) Oxygen and sulfur isotope fractionation during anaerobic bacterial disproportionation of elemental sulfur. *Geochimica et Cosmochimica Acta*, *65*, 1601–1609.

Brand, W.A., Coplen, T.B., Vogl, J., Rosner, M. & Prohaska, T. (2014) Assessment of international reference materials for isotope-ratio analysis (IUPAC Technical Report). *Pure and Applied Chemistry*, *86*, 425–467.

Burdett, J.W., Arthur, M.A. & Richardson, M. (1989) A Neogene seawater sulfur isotope age curve from calcareous pelagic microfossils. *Earth and Planetary Science Letters*, *94*, 189–198.

Casella, L.A., Griesshaber, E., Yin, X., Ziegler, A., Mavromatis, V., Müller, D. et al. (2017) Experimental diagenesis: Insights into aragonite to calcite transformation of *Arctica islandica* shells by hydrothermal treatment. *Biogeosciences*, *14*, 1461–1492.

Corrège, T. (2006) Sea surface temperature and salinity reconstruction from coral geochemical tracers. *Palaeogeography, Palaeoclimatology, Palaeoecology*, *232*, 408–428.

Cuif, J., Dauphin, Y., Doucet, J., Salome, M. & Susini, J. (2003) XANES mapping of organic sulfate in three scleractinian coral skeletons. *Geochimica et Cosmochimica Acta*, *67*, 75–83.

Cuif, J.P., Dauphin, Y. & Gautret, P. (1999) Compositional diversity of soluble mineralizing matrices in some recent coral skeletons compared to fine-scale growth structures of fibres: Discussion of consequences for biomineralization and diagenesis. *International Journal of Earth Sciences*, *88*, 582–592.

Dauphin, Y. (2003) Soluble organic matrices of the calcitic prismatic shell layers of two pteriomorphid bivalves *Pinna nobilis* and *Pinctada margaritifera*. *Journal of Biological Chemistry*, *278*, 15168–15177.

Dauphin, Y., Cuif, J., Doucet, J., Salomé, M., Susini, J. & Williams, C. (2003) In situ mapping of growth lines in the calcitic prismatic layers of mollusc shells using X-ray absorption near-edge structure (XANES) spectroscopy at the sulphur K-edge. *Marine Biology*, *142*, 299–304.

Dauphin, Y., Cuif, J.P., Salomé, M. & Susini, J. (2005) Speciation and distribution of sulfur in a mollusk shell as revealed by in situ maps using X-ray absorption near-edge structure (XANES) spectroscopy at the S K-edge. *American Mineralogist*, *90*, 1748–1758.

Fallon, S.J., White, J.C. & McCulloch, M.T. (2002) Porites corals as recorders of mining and environmental impacts: Misima Island, Papua New Guinea. *Geochimica Cosmochimica Acta*, *66*, 45–62.

Fichtner, V., Strauss, H., Mavromatis, V., Dietzel, M., Huthwelker, T., Borca, C.N. et al. (2018) Incorporation and subsequent diagenetic alteration of sulfur in *Arctica islandica*. *Chemical Geology*, *482*, 72–90.

Flank, A.M., Cauchon, G., Lagarde, P., Bac, S., Janousch, M., Wetter, R. et al. (2006) LUCIA, a microfocus soft XAS beamline. *Nuclear Instruments and Methods in Physics Research Section B: Beam Interactions with Materials and Atoms*, 246, 269–274.

Foriel, J., Philippot, P., Susini, J., Dumas, P., Somogyi, A., Salomé, M. et al. (2004) High-resolution imaging of sulfur oxidation states, trace elements, and organic molecules distribution in individual microfossils and contemporary microbial filaments. *Geochimica et Cosmochimica Acta*, 68, 1561–1569.

Gill, B.C., Lyons, T.W. & Saltzman, M.R. (2007) Parallel, high-resolution carbon and sulfur isotope records of the evolving Paleozoic marine sulfur reservoir. *Palaeogeography, Palaeoclimatology, Palaeoecology*, 256, 156–173.

Glover, C.P. & Kidwell, S.M. (1993) Influence of organic matrix on the post-mortem destruction of molluscan shells. *Journal of Geology*, 101, 729–747.

Hendy, E.J., Gagan, M.K. & Lough, J.M. (2003) Chronological control of coral records using luminescent lines and evidence for non-stationary ENSO teleconnections in northeast Australia. *The Holocene*, 13, 187–199.

Johnston, D.T., Gill, B.C., Masterson, A., Beirne, E., Casciotti, K.L., Knapp, A.N. et al. (2014) Placing an upper limit on cryptic marine sulphur cycling. *Nature*, 513, 530–533.

Kampschulte, A. & Strauss, H. (2004) The sulfur isotopic evolution of Phanerozoic seawater based on the analysis of structurally substituted sulfate in carbonates. *Chemical Geology*, 204, 255–286.

Kaplan, I.R. & Rittenberg, S.C. (1964) Microbiological fractionation of sulphur isotopes. *Microbiology*, 34, 195–212.

Karney, G.B., Butler, P.G., Speller, S., Scourse, J.D., Richardson, C.A., Schröder, M. et al. (2012) Characterizing the microstructure of *Arctica islandica* shells using NanoSIMS and EBSD. *Geochemistry, Geophysics, Geosystems*, 13, 4.

Lange, S.M. (2017) Microbial alteration of carbonate archives. Doctoral dissertation, GEOMAR Helmholtz Centre for Ocean Research, Kiel, Germany.

Lange, S.M., Krause, S., Ritter, A.-C., Fichtner, V., Immenhauser, A., Strauss, H. et al. (2018) Anaerobic microbial activity affects earliest diagenetic pathways of bivalve shells. *Sedimentology*, 65(4), 1390–1411. https://doi.org/10.1111/sed.12428

Lowenstam, H.A. & Weiner, S. (1989) *On biomineralization*. Oxford: Oxford University Press, 324 pp. ISBN: 0-19-504977-2.

Marin, F., Le Roy, N. & Marie, B. (2012) The formation and mineralization of mollusk shell. *Frontiers in Bioscience*, 4, 1099–1125.

Marshall, J.F. & McCulloch, M.T. (2002) An assessment of the Sr/Ca ratio in shallow water hermatypic corals as a proxy for sea surface temperature. *Geochimica et Cosmochimica Acta*, 66, 3263–3280.

Nguyen, L.T., Rahman, M.A., Maki, T., Tamenori, Y., Yoshimura, T., Suzuki, A. et al. (2014) Distribution of trace element in Japanese red coral *Paracorallium japonicum* by μ-XRF and sulfur speciation by XANES: Linkage between trace element distribution and growth ring formation. *Geochimica et Cosmochimica Acta*, 127, 1–9.

Paris, G., Fehrenbacher, J.S., Sessions, A.L., Spero, H.J. & Adkins, J.F. (2014) Experimental determination of carbonate-associated sulfate $\delta^{34}S$ in planktonic foraminifera shells. *Geochemistry, Geophysics, Geosystems*, 15, 1452–1461.

Peck, H.D. Jr & Lissolo, T. (1988) Assimilatory and dissimilatory sulphate reduction: Enzymology and bioenergetics. In: Cole, J.A. & Ferguson, S.J. (Eds.), *The nitrogen and sulphur cycles*. Cambridge: Cambridge University Press, pp. 99–132.

Pederson, C.L., Mavromatis, V., Dietzel, M., Rollion-Bard, C., Breitenbach, S.F.M., Yu, D. et al. (2020) Variation in the diagenetic response of aragonite archives to hydrothermal alteration. *Sedimentary Geology*, 406, 105716.

Pederson, C., Mavromatis, V., Dietzel, M., Rollion-Bard, C., Nehrke, G., Jöns, N. et al. (2019) Diagenesis of mollusc aragonite and the role of fluid reservoirs. *Earth and Planetary Science Letters*, 514, 130–142.

Perrin, J., Rivard, C., Vielzeuf, D., Laporte, D., Fonquernie, C., Ricolleau, A. et al. (2017) The coordination of sulfur in synthetic and biogenic Mg calcites: The red coral case. *Geochimica et Cosmochimica Acta*, 197, 226–244.

Pickering, I.J., Sneeden, E.Y., Prince, R.C., Block, E., Harris, H.H., Hirsch, G. et al. (2009) Localizing the chemical forms of sulfur in vivo using X-ray fluorescence spectroscopic imaging: Application to onion (*Allium cepa*) tissues. *Biochemistry*, 48(29), 6846–6853.

Pingitore, N.E., Meitzner, G. & Love, K.M. (1995) Identification of sulfate in natural carbonates by X-ray absorption spectroscopy. *Geochimica et Cosmochimica Acta*, 59, 2477–2483.

Ravel, B. & Newville, M. (2005) Athena, artemis, hephaestus: Data analysis for X-ray absorption spectroscopy using IFEFFIT. *Journal of Synchrotron Radiation*, 12, 537–541.

Richardson, J.A., Newville, M., Lanzirotti, A., Webb, S.M., Rose, C.V., Catalano, J.G. et al. (2019) The source of sulfate in brachiopod calcite: Insights from μ-XRF imaging and XANES spectroscopy. *Chemical Geology*, 529, 119328.

Schiff, J.A. & Fankhauser, H. (1981) Assimilatory sulfate reduction. In: *Biology of inorganic nitrogen and sulfur*. Heidelberg: Springer, Berlin, pp. 153–168.

Schöne, B.R. (2013) *Arctica islandica* (Bivalvia): a unique paleoenvironmental archive of the northern North Atlantic Ocean. *Global and Planetary Change*, 111, 199–225.

Schöne, B.R., Zhang, Z., Jacob, D., Gillikin, D.P., Tütken, T., Garbe-Schönberg, D. et al. (2010) Effect of organic matrices on the determination of the trace element chemistry (Mg, Sr, Mg/Ca, Sr/Ca) of aragonitic bivalve shells (*Arctica islandica*)—-Comparison of ICP-OES and LA-ICP-MS data. *Geochemistry Journal*, 44, 23–37.

Schöne, B.R., Zhang, Z., Radermacher, P., Thébault, J., Jacob, D.E., Nunn, E.V. et al. (2011) Sr/Ca and Mg/Ca ratios of ontogenetically old, long-lived bivalve shells (*Arctica islandica*) and their function as paleotemperature proxies. *Palaeogeography, Palaeoclimatology, Palaeoecology*, 302, 52–64.

Schurr, S.L., Genske, F., Strauss, H. & Stracke, A. (2020) A comparison of sulfur isotope measurements of geologic materials by inductively coupled plasma and gas source mass spectrometry. *Chemical Geology*, 558, 119869.

Sejrup, H.P. & Haugen, J.E. (1994) Amino acid diagenesis in the marine bivalve *Arctica islandica* Linné from northwest European sites: Only time and temperature? *Journal of Quaternary Science*, 9, 301–309.

Shirai, K., Schöne, B.R., Miyaji, T., Radarmacher, P., Krause, R.A. & Tanabe, K. (2014) Assessment of the mechanism of elemental incorporation into bivalve shells (*Arctica islandica*) based on elemental distribution at the microstructural scale. *Geochimica et Cosmochimica Acta*, 126, 307–320.

Solé, V.A., Papillon, E., Cotte, M., Walter, P. & Susini, J. (2007) A multiplatform code for the analysis of energy-dispersive X-ray fluorescence spectra. *Spectrochimica Acta Part B: Atomic Spectroscopy*, 62, 63–68.

Staudt, W.J. & Schoonen, M.A. (1995) Sulfate incorporation into sedimentary carbonates. In ACS Symposium Series, 612. Washington, DC, pp. 332–347. https://doi.org/10.1021/bk-1995-0612.ch018

Takano, B. (1985) Geochemical implications of sulfate in sedimentary carbonates. *Chemical Geology*, *49*, 393–403.

Tamenori, Y., Yoshimura, T., Luan, N.T., Hasegawa, H., Suzuki, A., Kawahata, H. et al. (2014) Identification of the chemical form of sulfur compounds in the Japanese pink coral (*Corallium elatius*) skeleton using μ-XRF/XAS speciation mapping. *Journal of Structural Biology*, *186*, 214–223.

Thamdrup, B., Finster, K., Hansen, J.W. & Bak, F. (1993) Bacterial disproportionation of elemental sulfur coupled to chemical reduction of iron and manganese. *Applied and Environmental Microbiology*, *59*, 101–108.

Wanamaker, A.D. Jr, Baker, A., Butler, P.G., Richardson, C.A., Scourse, J.D., Ridgway, I. et al. (2009) A novel method for imaging internal growth patterns in marine mollusks: A fluorescence case study on the aragonitic shell of the marine bivalve *Arctica islandica* (Linnaeus). *Limnology and Oceanography: Methods*, *7*, 673–681.

Weiner, S. (1984) Organization of organic matrix components in mineralized tissues. *American Zoologist*, *24*, 945–951.

Weiner, S. & Addadi, L. (1991) Acidic macromolecules of mineralized tissues: the controllers of crystal formation. *Struct. Chem.*, *16*, 252–256.

Wotte, T., Shields-Zhou, G.A. & Strauss, H. (2012) Carbonate-associated sulfate: Experimental comparisons of common extraction methods and recommendations toward a standard analytical protocol. *Chemical Geology*, *326*, 132–144.

Zhao, J.S., Manno, D., Beaulieu, C., Paquet, L. & Hawari, J. (2005) *Shewanella sediminis sp*. nov., a novel Na+- requiring and hexahydro-1,3,5-trinitro-1,3,5-triazine-degrading bacterium from marine sediment. *International Journal of Systematic and Evolutionary Microbiology*, *55*, 1511–2152.

SUPPORTING INFORMATION

Additional supporting information may be found online in the Supporting Information section.

How to cite this article: Fichtner V, Lange SM, Krause S, et al. Microbial activity affects sulphur in biogenic aragonite. *Depositional Rec*. 2021;7:500–519. https://doi.org/10.1002/dep2.133